Chapter 3

Rock Strength and Failure Criteria

Whenever we place an engineered structure against rock, we ask the following two questions: Will the *stresses in the rock* reach the maximum levels that are tolerable, with consequent local or gross rock failure? Will the *displacements of the rock* under the loads to be applied produce such large strains in the structure that they cause its damage or destruction? This chapter discusses the first question. Assuming that we can estimate the initial stresses in the rock mass and that we can predict how these stresses will be modified by the construction and operation of the engineering work, how may we discover if the rock will flow, yield, crush, crack, buckle, or otherwise give way in service? For this we utilize "criteria of failure"—equations that link the limiting combinations of stress components separating acceptable from inadmissible conditions. Before we can propose meaningful criteria, however, we should examine how rocks usually fail, that is, whether in bending, shearing, crushing, or otherwise.

3.1 Modes of Rock Failure

The varieties of load configurations in practice are such that no single mode of rock failure predominates. In fact, flexure, shear, tension, and compression can each prove most critical in particular instances. *Flexure* refers to failure by bending, with development and propagation of tensile cracks. This may tend to occur in the layers above a mine roof (Figure 3.1*a*). As the "immediate roof" detaches from the rock above, under gravity, a gap forms and a beam of rock sags downward under its own weight. As the beam begins to crack, its neutral axis advances upward; eventually, the cracks extend right through the beam, after which sections of rocks may come loose and fall. Flexural failure can also

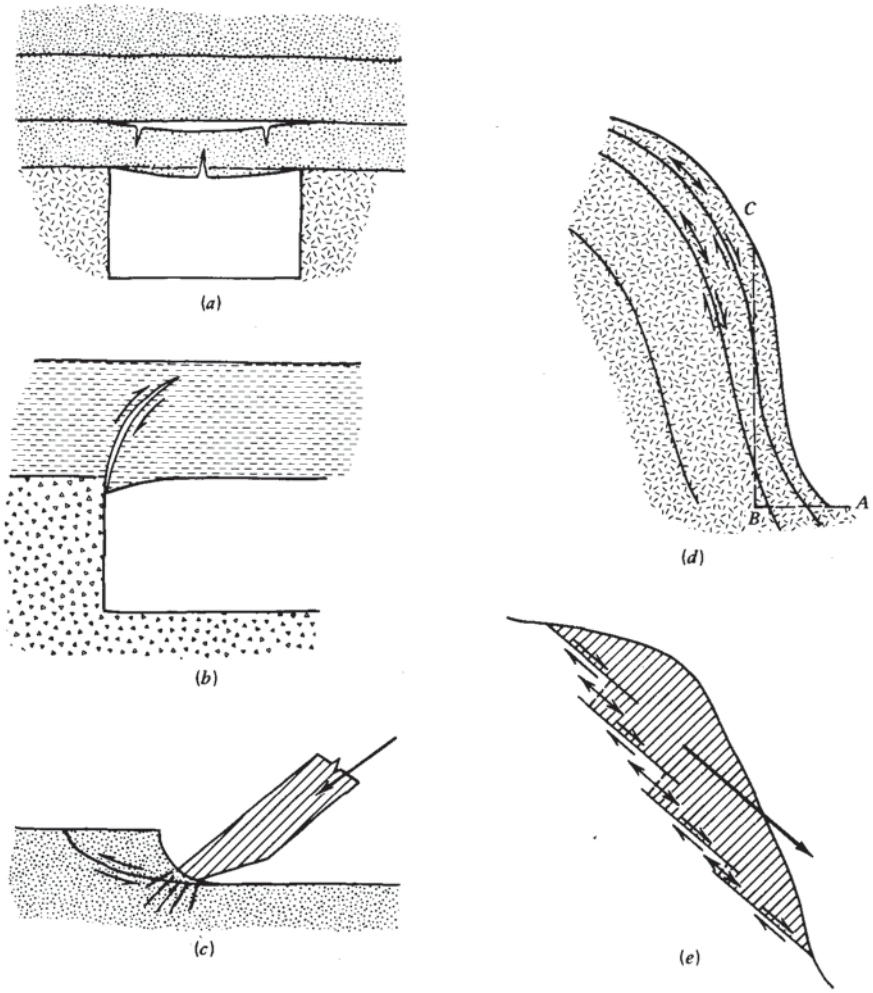

Figure 3.1 Examples of failure modes involving breakage of rock. (*a*) Flexure. (*b*) Shear. (*c*) Crushing and tensile cracking, followed by shear. (*d* and *e*) Direct tension.

occur in rock slopes with steeply dipping layers as the layers overturn toward the free space ("toppling failure").

Shear failure refers to formation of a surface of rupture where the shear stresses have become critical, followed by release of the shear stress as the rock suffers a displacement along the rupture surface. This is common in slopes cut in weak, soil-like rocks such as weathered clay shales and crushed rock of fault zones. It may occur in a mine with stiff ore and a softer, weaker roof or floor; the shear stresses in the roof or pillar base can allow the pillar to

"punch" relatively upward into the roof (Figure 3.1*b*) or downward into the floor. Rock cutters employing "drag bits" or "picks" owe their cutting action partly to shear along fractures caused by compression under the edge of the bit (Figure 3.1*c*). The vibration of such cutters as they advance reflects the periodic formation and removal of rock chips.

Direct tension is occasionally set up in rock layers resting on convex upward slope surfaces (e.g., in sheeted granites (Figure 3.1*d*)) and in sedimentary rocks on the flank of an anticline. The base of the slope has layers inclined more steeply than friction will allow and the balance of support for the weight of the layers is the tensile pull from the stable part of the slope above. Direct tension also is the mechanism of failure in rock slopes with nonconnected, short joint planes; the formation of tension cracks severs the rock bridges and allows a complete block of rock to translate downward en masse (Figure 3.1*e*). When rock breaks in tension, the surface of rupture is rather rough and free from crushed rock particles and fragments. With shear failure, on the contrary, the surface of failure is slick and there is much powder from crushing and communition of rock. Direct tension failure also occurs when the circumference of a borehole or a tunnel is stretched owing to internal water or gas pressure. The former situation arises when a pressure tunnel is operated at excessive pressure and when a drill hole is "hydraulically fractured" by pumping water to a high pressure in a section isolated by "packers." Detonation of an explosive agent in a borehole will raise gas pressure against the wall to millions of pounds per square inch; tensile failure then creates a series of radial cracks beyond the immediate periphery of the borehole, which may be crushed or in extreme cases actually melted. Some extension joints in bedrock are believed to have arisen from circumferential strain accompanying large amounts of uplift over broad geographic belts ("epeirogeny").

Crushing or *compression failure* occurs in intensely shortened volumes or rock penetrated by a stiff punch. Examination of processes of crushing shows it to be a highly complex mode, including formation of tensile cracks and their growth and interaction through flexure and shear. When the particles and slivers formed by cracking are not free to move away from the zone of compression, they become finely comminuted. This happens under some drill bits and under disk cutters of boring machines. In a mine pillar, overextraction of ore can lead to pillar failure by splitting and shear, although the destruction of the load-carrying capacity of the pillar through growth and coalescence of cracks is sometimes spoken of as "compression failure."

It may be appreciated that the actual destruction of a load-carrying rock mass is rather complex and involves one or more of the modes mentioned. It is no wonder then that no single method of testing rock has been advanced to the exclusion of others. In fact, the theory of failure makes use of a variety of laboratory and field testing techniques adapted to the special nature of the problem at hand.

3.2 Common Laboratory Strength Tests

To characterize the strength of rock specimens, unconfined and confined compression tests, shear tests, and direct and indirect tension tests are used widely. Other test configurations are preferred for special applications and a great variety of procedures has been investigated. We review here the important features of the most widely used tests—unconfined compression, triaxial compression, splitting tension ("Brazilian tests"), beam bending, and ring shear. Figure 3.2 shows rock preparation equipment required to prepare specimens for such tests.

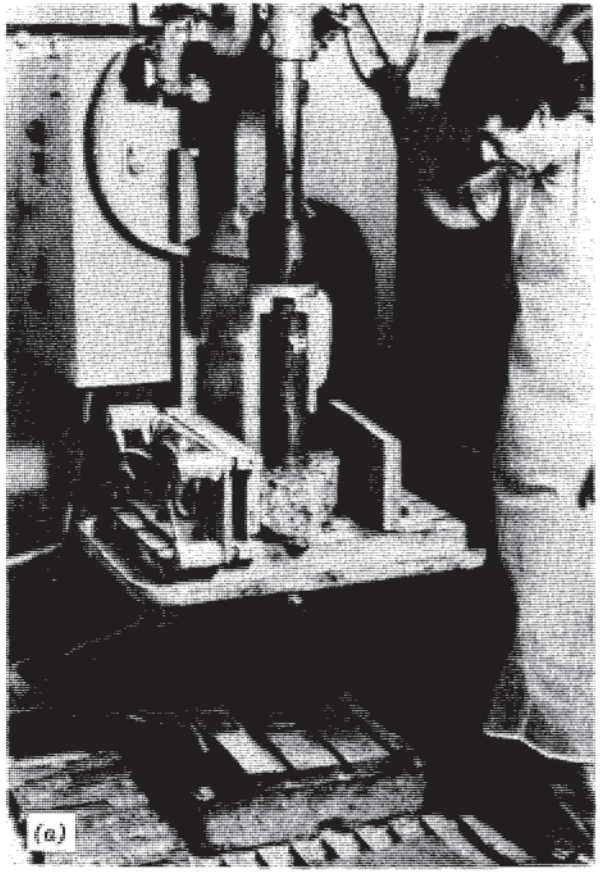

Figure 3.2 Equipment for preparing rock specimens for laboratory tests. (*a*) A drill press modified for feed under constant pressure and equipped with a vise to retain arbitrary blocks during drilling. (The drill press was devised by Quentin Gorton.)

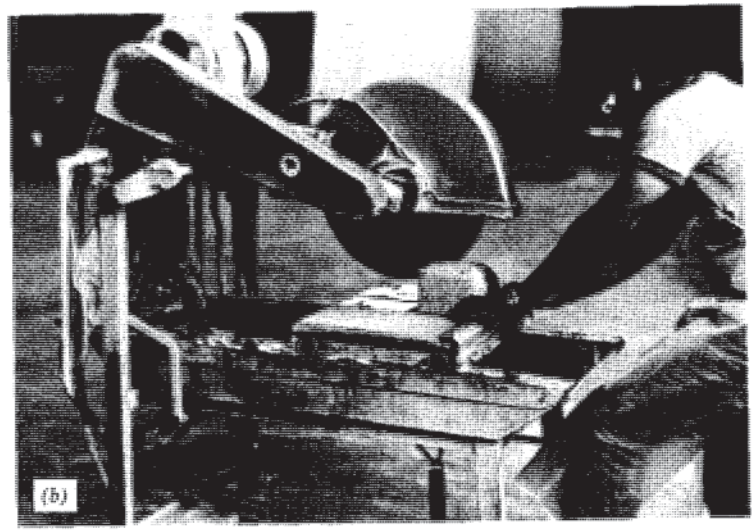

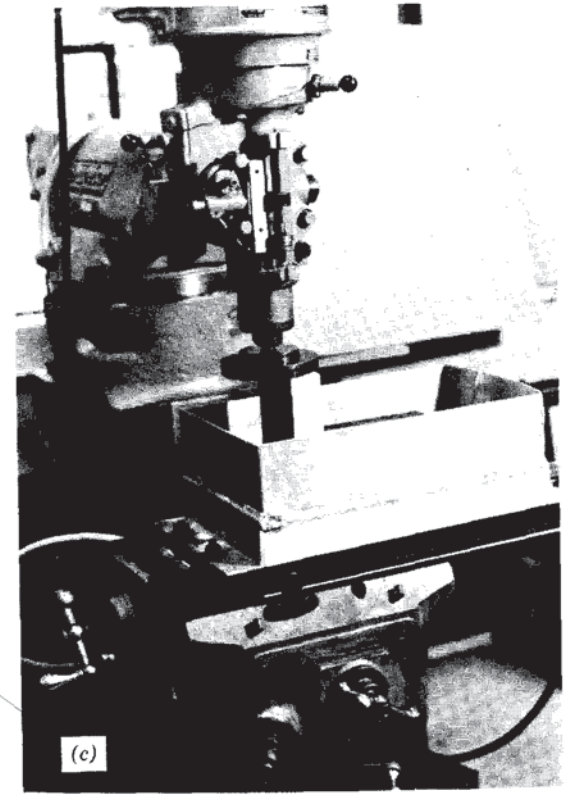

Figure 3.2 Equipment for preparing rock specimens for laboratory tests. (*b*) A diamond saw. (*c*) A surface grinder adapted from a milling machine by adding a diamond wheel and water bath.

Unconfined compression (Figure 3.3*a*) is the most frequently used strength test for rocks, yet it is not simple to perform properly and results can vary by a factor of more than two as procedures are varied. The test specimen should be a rock cylinder of length-to-width ratio in the range 2 to 2.5 with flat, smooth, and parallel ends cut perpendicularly to the cylinder axis. Procedures are recommended in ASTM designation D2938-71a and by Bieniawski and Bernede (1979). Capping of the ends with sulfur or plaster to specified smoothness is thought to introduce artificial end restraints that overly strengthen the rock. However, introduction of Teflon pads to reduce friction between the ends and the loading surfaces can cause outward extrusion forces producing a premature splitting failure, especially in the harder rocks. When mine pillars are studied, it is sometimes preferable to machine the compression specimen from a large cylinder to achieve loading through rock of the upper and lower regions into the more slender central region. In the standard laboratory compression test, however, cores obtained during site exploration are usually trimmed and compressed between the crosshead and platen of a testing machine. The compressive strength q_u is expressed as the ratio of peak load P to initial cross-sectional area A:

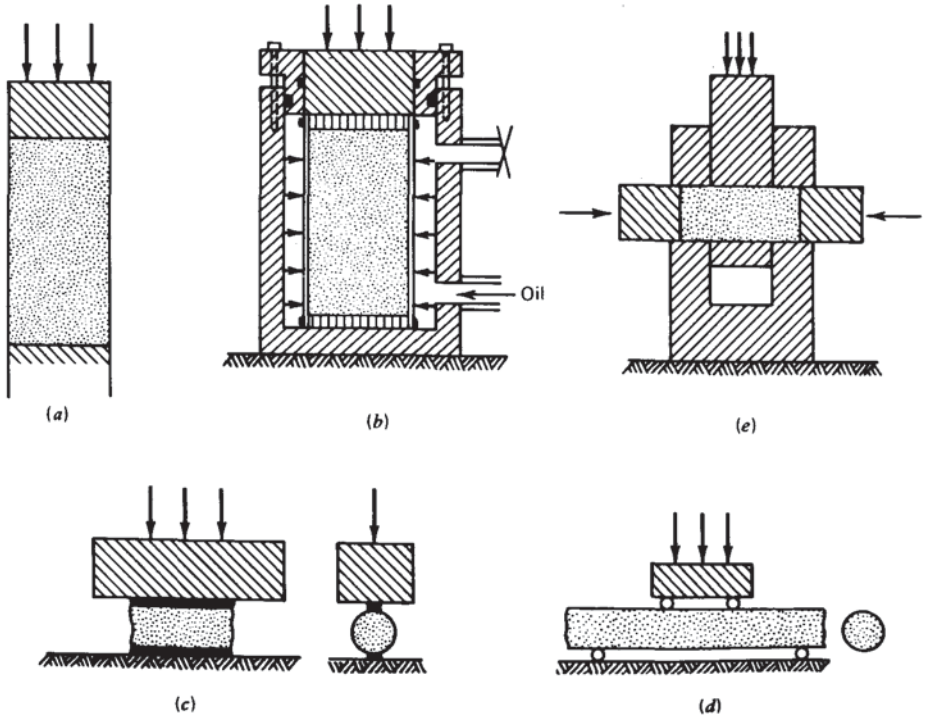

Figure 3.3 Common laboratory tests for characterizing rock strength criteria. (*a*) Unconfined compression. (*b*) Triaxial compression. (*c*) Splitting tension (Brazilian). (*d*) Four-point flexure. (*e*) Ring shear.

$$q_u = \frac{P}{A} \tag{3.1}$$

Representative values of q_u are listed in Table 3.1.

Triaxial compression (Figure 3.3*b*) refers to a test with simultaneous compression of a rock cylinder and application of axisymmetric confining pressure. Recommended procedures are described in ASTM designation D2664-67 (1974) and in an ISRM Committee report by Vogler and Kovari (1978).

Table 3.1 *Unconfined Compressive Strength* (q_u) *and Ratio of Compressive to Indirect Tensile Strength* (q_u/T_0) *for Specimens of Representative Rocks*

Description[a]	q_u MPa	q_u psi	q_u/T_0[b]	Reference[c]
Berea sandstone	73.8	10,700	63.0	5
Navajo sandstone	214.0	31,030	26.3	5
Tensleep sandstone	72.4	10,500		1
Hackensack siltstone	122.7	17,800	41.5	5
Monticello Dam s.s. (greywacke)	79.3	11,500		4
Solenhofen limestone	245.0	35,500	61.3	5
Bedford limestone	51.0	7,400	32.3	5
Tavernalle limestone	97.9	14,200	25.0	5
Oneota dolomite	86.9	12,600	19.7	5
Lockport dolomite	90.3	13,100	29.8	5
Flaming Gorge shale	35.2	5,100	167.6	3
Micaceous shale	75.2	10,900	36.3	2
Dworshak Dam gneiss				
45° to foliation	162.0	23,500	23.5	5
Quartz mica schist ⊥ schistocity	55.2	8,000	100.4	5
Baraboo quartzite	320.0	46,400	29.1	5
Taconic marble	62.0	8,990	53.0	5
Cherokee marble	66.9	9,700	37.4	5
Nevada Test Site granite	141.1	20,500	12.1	7
Pikes Peak granite	226.0	32,800	19.0	5
Cedar City tonalite	101.5	14,700	15.9	6
Palisades diabase	241.0	34,950	21.1	5
Nevada Test Site basalt	148.0	21,500	11.3	7
John Day basalt	355.0	51,500	24.5	5
Nevada Test Site tuff	11.3	1,650	10.0	7

[a] Description of rocks listed in Table 3.1:

Berea sandstone, from Amherst, Ohio; fine grained, slightly porous; cemented. *Navajo sandstone*, from Glen Canyon Dam site, Arizona; friable, fine to medium grained. (Both sandstones are

Table Footnote (*continued*)

predominately composed of quartz grains.) *Tensleep sandstone*, Pennsylvanian-age sandstone from Alcova Powerhouse, Wyoming, (near Casper); calcite cemented; medium grained. *Hackensack siltstone*, New Jersey; from Triassic Newark Series; cemented with hematite; argillaceous. *Monticello Dam greywacke*, Cretaceous sandstone from the Monticello dam foundation, California; medium to coarse grained, cemented feldspar, quartz, and other components; some feldspars altered to mica. *Solenhofen limestone*, from Bavaria; very fine, interlocked crystalline texture. *Bedford limestone*, Indiana; slightly porous, oolitic, bioclastic limestone. *Tavernalle limestone*, from Carthage, Missouri; fine grained, cemented and interlocked crystalline limestone with fossils. *Oneota dolomite*, Kasota, Minnesota; fine-grained interlocking granular texture with mottled appearance due to disseminated calcite veins. *Lockport dolomite*, Niagara Falls, New York; very fine-grained cemented granular texture grading to interlocking crystalline texture; some anhydrite grains. *Flaming Gorge shale*, from Flaming Gorge damsite, Utah, Wyoming border. *Micaceous shale*, from the Jonathan mine, Ohio; the clay mineral is kaolinite. *Dworshak dam gneiss*, from Orofino, Idaho; fine to medium-grained granodiorite gneiss with prominent foliation. *Quartz mica schist* with crenulated schistocity; origin unknown. *Baraboo quartzite*, from Wisconsin; fine-grained, brittle, massive Pre-Cambrian quartzite with tightly interlocking crystalline texture. *Taconic white marble*, Rutland, Vermont; uniform, fine-grained massive marble, with sugary texture. *Cherokee marble*, from Tate, Georgia; medium- to coarse-grained massive marble with tightly interlocking crystalline texture. *Nevada Test Site* "granite," granodiorite from Piledriver Experiment; coarse-grained. *Pikes Peak granite*, Colorado Springs, Colorado; fine- to medium-grained dense; interlocked crystalline texture. *Cedar City tonalite*, somewhat weathered quartz monzonite, with porosity of 4.9%, from Cedar City, Utah. *Palasades diabase*, from West Nyack, New York; medium-grained. *Nevada Test Site basalt*, from Buckboard Mesa; fine, olivine basalt. *John Day basalt*, from John Day dam site, Arlington, Oregon. *Nevada Test Site tuff*, from "Red Hot" experiment; welded volcanic ash; porosity 19.8%.

[b] Tensile strengths were determined by point load tests for all entries corresponding to reference 5; determined by Brazilian test for entries corresponding to references 6 and 7. The point load tensile strength T_0 in megapascals was calculated from the load at failure (F), in meganewtons for point loading across the rock core diameter (d), in meters; $T_0 = 6.62\ 10^{-3}\ F/d^2$ (Reichmuth, 1963).

[c] References for Table 3.1:

General

Kulhawy, F. (1975) cited in references at the end of this chapter.
Lama, R. D. and Vutukuri, V. S., cited in references in Chapter 1.

Specific

1. Balmer, G. G. (1953) Physical properties of some typical foundation rocks, U. S. Bureau of Reclamation Concrete Lab Report SP-39.
2. Blair, B. E. (1956) Physical properties of mine rock, Part IV, U. S. Bureau of Mines Rep. Inv. 5244.
3. Brandon, T. R. (1974) Rock mechanic properties of typical foundation rocks, U. S. Bureau of Reclamation Rep. REC-ERC 74-10.
4. Judd, W. R. (1969) Statistical methods to compile and correlate rock properties, Purdue University, Department of Civil Engineering.
5. Miller, R. P. (1965) Engineering classification and index properties for intact rock, Ph.D. Thesis, University of Illinois.
6. Saucier, K. L. (1969) Properties of Cedar City tonalite, U. S. Army Corps of Engineers, WES Misc. Paper C-69-9.
7. Stowe, R. L. (1969) Strength and deformation properties of granite, basalt, limestone, and tuff, U. S. Army Corps of Engineers, WES Misc. Paper C-69-1.

At the peak load, the stress conditions are $\sigma_1 = P/A$ and $\sigma_3 = p$, where P is the highest load supportable parallel to the cylinder axis, and p is the pressure in the confining medium. The confinement effect, that is, the strengthening of the rock by the application of confining pressure p, is realized only if the rock is enclosed in an impervious jacket. The confining fluid is normally hydraulic oil and the jacket is oil-resistant rubber (e.g., polyurethane); for tests of short duration, bicycle inner tube is suitable. Most rocks show a considerable strengthening effect due to confining pressure and it has become routine to conduct triaxial compression tests on rocks.

Many varieties of triaxial cells are in use in rock mechanics laboratories and several types are available from commercial suppliers. Figure 3.4*a* shows two cells used at the University of California, Berkeley. The one on the left was designed by Owen Olsen for the U. S. Bureau of Reclamation. It provides extra room for inserting instruments and gages and is easily adapted for pore pressure and other special measurements; however, the diameter of the piston is considerably larger than the diameter of the specimen, with the result that a large uplift force from the confining pressure must be reacted by the axial loading machine. The chamber on the right, based on a design by Fritz Rummel, avoids this problem. The rock specimen, with strain gages attached, will be jacketed before insertion in the triaxial chamber. Figure 3.4*b* shows a high-pressure, high-temperature triaxial test facility at the TerraTek Laboratory, Salt Lake City, Utah. This computer-controlled apparatus can supply confining

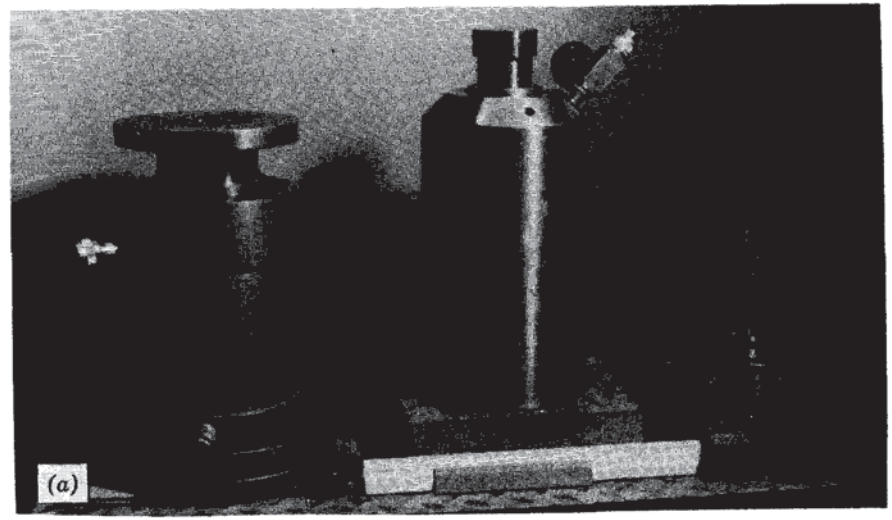

Figure 3.4 Equipment for triaxial compression tests. (*a*) Two types of cells used at Berkeley.

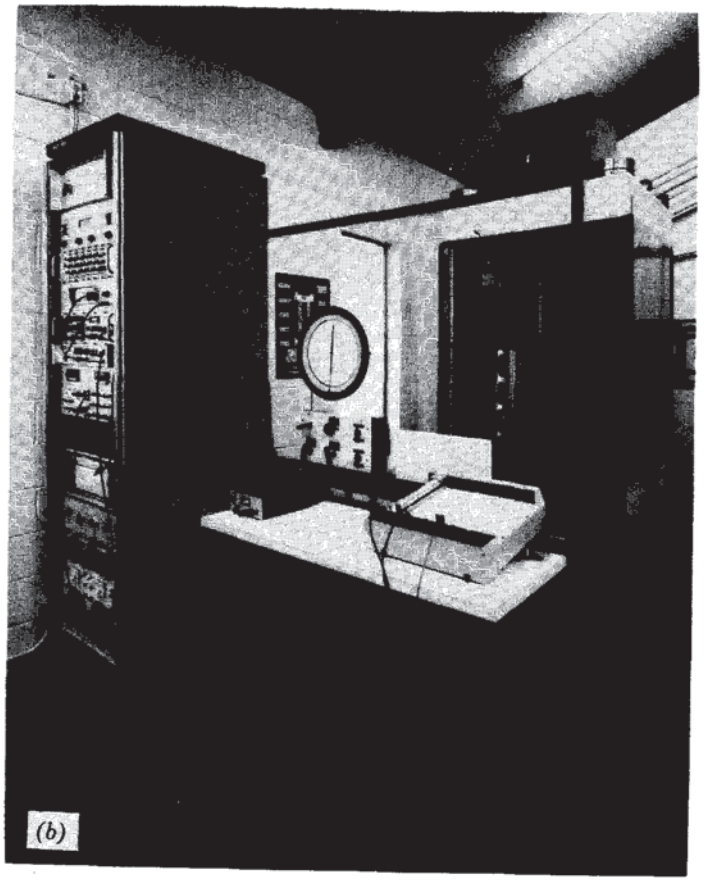

Figure 3.4 Equipment for triaxial compression tests. (*b*) A high-pressure, high-temperature facility at TerraTek, Salt Lake City, Utah.

pressures up to 200 MPa to specimens as large as 10 cm in diameter at temperatures as high as 200°C (5-cm-diameter specimens can be heated up to 535°C).

The usual procedure for conducting a triaxial compression test is first to apply the confining pressure all round the cylinder (i.e., $\sigma_1 = \sigma_3 = p$) and then to apply the axial load $\sigma_1 - p$ as the lateral pressure is held constant. In this case, the triaxial compression experiment can be interpreted as the superposition of a uniaxial compression test on an initial state of all-round compression. However, the actual path of loading in service may be quite different; since some rocks demonstrate strong path effects it may then be desirable to follow different procedures. For example, the stresses in the rock at the front of a traveling plane wave are applied simultaneously in all directions. With computer or manual feedback control, it is possible to follow almost any prescribed path of loading, although, as will be shown later, not all paths can result in fracture under load. For the best results and a clear interpretation of the effects of load, both the axial shortening, and the lateral expansion of the specimen should be monitored during loading as discussed later.

The *Brazilian test*, described for cylindrical concrete specimens in ASTM designation C496-71,[1] is convenient for gaining an estimate of the tensile strength of rock. It has been found that a rock core about as long as its diameter will split along the diameter and parallel to the cylinder axis when loaded on its side in a compression machine (Figure 3.2*c*). The reason for this can be demonstrated by examining the stress inside a disk loaded at opposite sides of a diametral plane. In such a configuration the horizontal stresses perpendicular to the loaded diameter are uniform and tensile with magnitude

$$\sigma_{t,B} = \frac{2P}{\pi dt} \tag{3.2}$$

where P is the compression load, d is the cylinder diameter, and t is the thickness of the disk (the length of the cylinder). It is much easier to perform this type of test than to arrange the precise alignment and end preparation required for a direct tensile test.

The "Brazilian tensile strength" is estimated from the test result by reporting the value of $\sigma_{t,B}$ corresponding to the peak compression load. It should be understood, however, that the actual cause of failure may also reflect the action of the vertical stress along the vertical diameter in concert with the horizontal tension; the vertical stress is nonuniform increasing from a compressive stress of three times $\sigma_{t,B}$ at the center of the disk to progressively higher values as the ends are approached. According to the Griffith theory of failure, the critical point ought to be the center where the ratio of compression to tension is 3. With a principal stress ratio of 3, failure ought to result from the application of the tensile stress alone, without any complication from the simultaneous compression parallel to the eventual rupture plane. In fact, the Brazilian test has been found to give a tensile strength higher than that of the direct tension test, probably owing to the effect of fissures. Short fissures weaken a direct tension specimen more severely than they weaken a splitting tension specimen. The ratio of Brazilian to direct tensile strength has been found to vary from unity to more than ten as the length of preexisting fissures grows larger (Tourenq and Denis, 1970).

A *flexural test* causes failure of a rock beam by bending. Like the Brazilian test, flexural tests also can be run on rock cores lacking machined ends. Four-point flexural loading (Figure 3.3*d*), with the bottom of the core supported on

[1] Standard Method of Test for Splitting Tensile Strength of Cylindrical Concrete Specimens, ASTM Committee C-9 on Concrete and Concrete Aggregate.

points near the ends and the top of the core loaded from above at the third points, produces uniform moment in the central third of the specimen and gives better reproducibility of results than three-point loading in which the upper load is central. The flexural strength or "modulus of rupture" is the maximum tensile stress on the bottom of the rock corresponding to peak load. It is calculated from simple beam theory assuming elastic conditions throughout. The flexural strength is found to be two to three times as great as the direct tensile strength. For four-point bending of cylindrical rock specimens, with loads applied at $L/3$ from each end and reactions at the ends, the modulus of rupture (MR) is:

$$T_{MR} = \frac{16P_{max}L}{3\pi d^3} \tag{3.3}$$

where P_{max} is the maximum load, L is the length between load reactions on the lower surface, and d is the diameter of the core.

The *ring shear test* (Figure 3.3*e*) provides a relatively simple method to test intact rock strength as a function of confining pressure (Lundborg, 1966). In contrast to compression tests, core specimens for the ring shear test do not require perfectly square and smooth ends. As with the triaxial test, the results permit an appreciation of the rate of increase of strength with confining pressure. The latter is provided by the load parallel to the axis of the core. Two sets of complex fracture surfaces form along the two planes of imposed shear as the load is applied to the plunger.

If P is the peak load on the plunger, the peak shear stress (τ_p) is called the "shear strength" and is calculated by

$$\tau_p = \frac{P}{2A} \tag{3.4}$$

where A is the area across the core sample.

3.3 Stress-Strain Behavior in Compression

STRESS AND STRAIN

In discussing the deformations of rock undergoing compression from various directions, it proves useful to divide the stresses into two parts. *Nondeviatoric stresses* (σ_{mean}) are compressions equally applied in all directions, that is, a hydrostatic state of stress. *Deviatoric* stresses (σ_{dev}) are the normal and shear stresses that remain after subtracting a hydrostatic stress, equal to the mean normal stress, from each normal stress component. In the triaxial compression experiment, for example, the principal stresses are $\sigma_1 = P/A$ and $\sigma_2 = \sigma_3 = p$.

The nondeviatoric stress is given by $\frac{1}{3}(\sigma_1 + 2p)$ all around while the deviatoric stress is then what remains: $\sigma_{1,dev} = \frac{2}{3}(\sigma_1 - p)$ and $\sigma_{3,dev} = \sigma_{2,dev} = -\frac{1}{3}(\sigma_1 - p)$. There is strong motivation for doing this: deviatoric stress produces distortion and destruction of rocks while nondeviatoric stresses generally do not (as discussed in the next section). In the triaxial test, the initial pressuring is nondeviatoric; subsequently, both deviatoric and nondeviatoric stresses are raised simultaneously.

Normal strains in a triaxial compression specimen can be measured with surface-bonded electric resistance strain gages. A gage parallel to the specimen axis records the longitudinal strain $\varepsilon_{axial} = \Delta l/l$, while a strain gage affixed to the rock surface in the circumferential direction yields the lateral strain $\varepsilon_{lateral} = \Delta d/d$, where d is the diameter of the rock and l is its length (see Figure 3.4*a*). Assuming that the strain gage readings are zeroed after the confining pressure has been applied, we can write

$$\varepsilon_{lateral} = -\nu\varepsilon_{axial} \tag{3.5}$$

in which the constant of proportionality ν is called *Poisson's ratio*. In fact, proportionality is maintained only in the restricted range of loading during which there is no initiation and growth of cracks. For linearly elastic and isotropic rocks, ν must lie in the range 0 to 0.5 and is often assumed equal to 0.25. Because a rock expands laterally as its shortens axially (Figure 3.5), a negative sign is introduced to define Poisson's ratio as a positive quantity. For strains of less than several %, the volume change per unit of volume, $\Delta V/V$, is

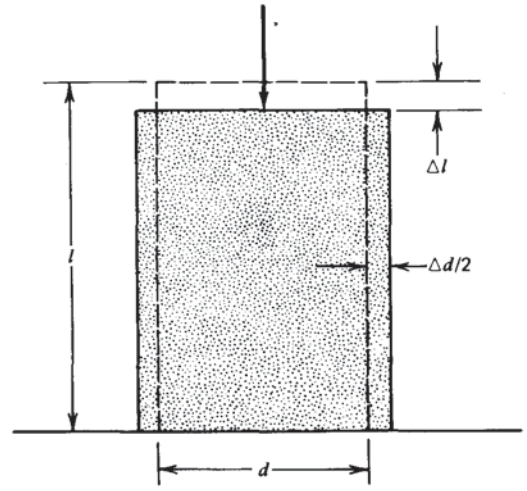

Figure 3.5 Deformations in compression tests.

closely approximated by the algebraic sum of the three normal strains. In the triaxial compression experiment then,

$$\frac{\Delta V}{V} = \varepsilon_{\text{axial}} + 2\varepsilon_{\text{lateral}}$$

or

$$\frac{\Delta V}{V} = \varepsilon_{\text{axial}}(1 - 2\nu) \tag{3.6}$$

Volumetric strain produced either by deviatoric or nondeviatoric stresses can be measured indirectly using surface strain gages and applying Equation 3.5 or directly by monitoring the flow of oil into or out of the confining vessel as the confining pressure is held constant by a servomechanism.

HYDROSTATIC COMPRESSION

Applying a nondeviatoric stress to a rock produces a volume decrease and eventually changes the rock fabric permanently, as pores are crushed. However, it cannot produce a peak load response; that is, the rock can always accept an added increment of load, apparently for as high a pressure as one can generate. Tests have been conducted into the megabar region (millions of psi) producing phase changes in the solid. The pressure, volumetric strain curve is generally concave upward as shown in Figure 3.6 with four distinct regions. In the first, which may be the principal region for many good rocks in civil engineering service, preexisting fissures are closed and the minerals are slightly compressed. When the load is removed, most of the fissures remain closed and there is a net deformation or "per-def." The fissure porosity is related to the per-def.

After most of the fissures have closed, further compression produces bulk rock compression, consisting of pore deformation and grain compression at an approximately linear rate. The slope of the pressure-volumetric strain curve in this region is called the *bulk modulus*,[2] K. In porous rocks like sandstone, chalk, and clastic limestone, the pores begin to collapse due to stress concentrations around them; in well-cemented rocks, this may not occur until reaching a pressure of the order of 1 kbar (100 MPa or 14,500 psi), but in poorly or weakly cemented rocks, pore crushing can occur at much lower pressures. Finally, when all the pores have been closed, the only compressible elements remaining are the grains themselves and the bulk modulus becomes progressively higher. Nonporous rocks do not demonstrate pore "crush up" but show uniformly concave-upward deformation curves to 300 kbar or higher. Pore

[2] The compressibility C is $1/K$.

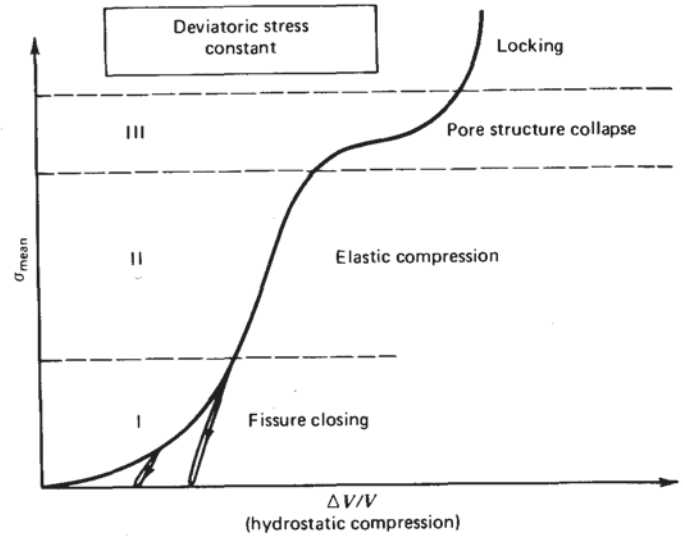

Figure 3.6 Volumetric compression under increasing mean stress, with constant deviatoric stress.

crushing is destructive in very porous rocks like chalk and pumice, which are converted to a cohesionless sediment on removal from the test chamber.

DEVIATORIC COMPRESSION

Applying deviatoric stress produces strikingly different results as shown in Figure 3.7. With initial application of the deviatoric stress, fissures and some pores begin to close, producing an inelastic, concave-upward stress-strain section. In most rocks, this is followed by linear relationships between axial stress and axial strain and between axial stress and lateral strain. At point B (Figure 3.7*a*), the rate of lateral strain begins to increase relative to the rate of axial strain (Poisson's ratio increases) as new cracks begin to form inside the most critically stressed portions of the specimen—usually near the sides of the midsection. A microphone attached to the rock will begin to pick up "rock noise" as new cracks form and old ones extend parallel to the direction of σ_1. In the region between stress B and stress C, cracks are considered to be "stable" meaning that with each increment of stress they grow to a finite length, and then stop growing. After point C, cracks that form propagate to the edges of the specimen and a system of intersecting, coalescing cracks is developed, which eventually form a semicontinuous rupture surface termed a "fault." Figures 3.7*c* and *d*, from Wawersik and Brace (1971), show this development. Bieniawski (1967a, b) suggested that point C corresponds to the yield point in

the axial stress-axial strain curve. The peak load, point D, is the usual object of failure criteria. However, the rock may not fail when the load reaches this point, as is discussed later. In a stiff loading system, it is possible to continue to shorten the specimen, as long as stress is reduced simultaneously. If the volumetric strain is plotted against the deviatoric stress as in Figure 3.7*b*, it is seen that the attainment of the crack initiation stress (B) is marked by a beginning of an increase in volume associated with sliding and buckling of rock slivers between cracks and opening of new cracks. At a stress level corresponding to stress point C, the specimen may have a bulk volume larger than at the start of the test. This increase in volume associated with cracking is termed *dilatancy*.

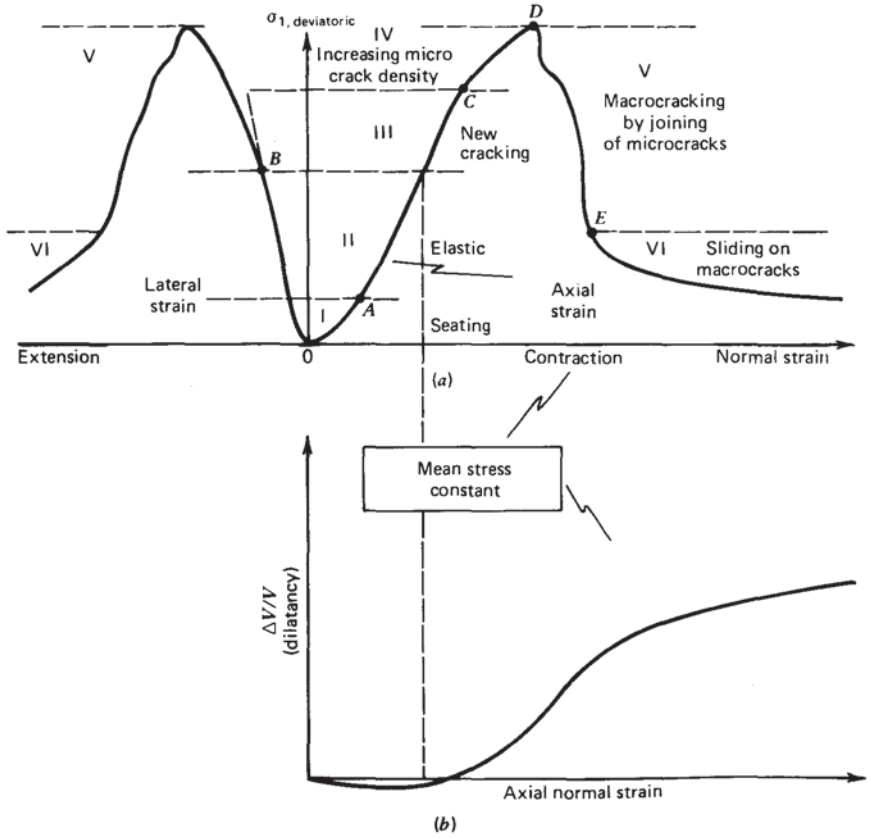

Figure 3.7 Deformation under increasing deviatoric stress, with constant mean stress (hypothetical curves). (*a*) Axial and lateral normal strain with increasing deviatoric axial stress. (*b*) Volumetric strain with increasing axial normal strain (dilatancy).

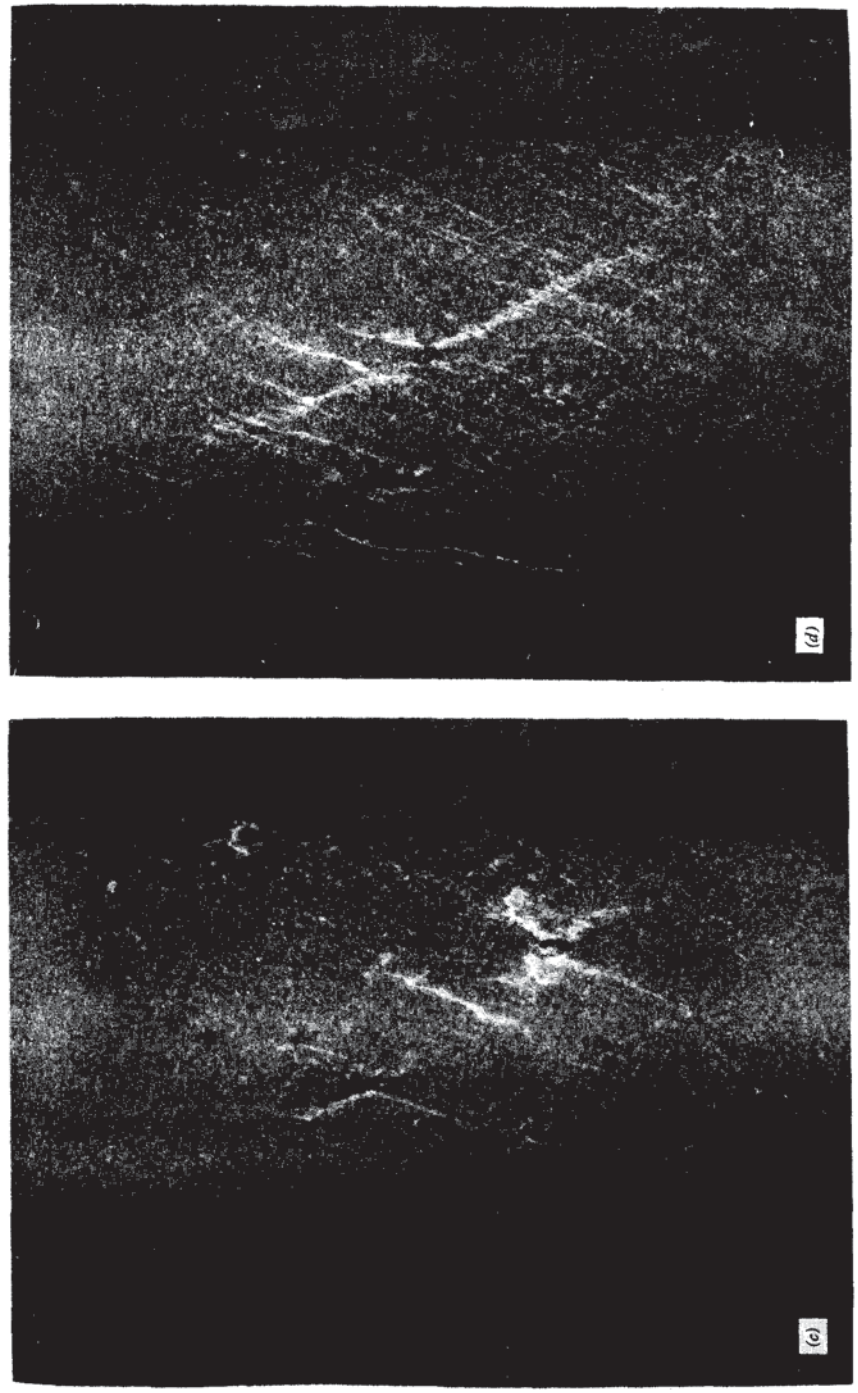

Figure 3.7 Deformation under increasing deviatoric stress, with constant mean stress (hypothetical curves). (*c*) at the peak axial stress; (*d*) just after the peak showing linkup of fractures to form a rupture surface. *c* and *d* Fractures formed in diabase during triaxial compression at 500 psi, reproduced from Wawersik and Brace (1971) with permission.

EFFECT OF CONFINING PRESSURE

Most rocks are significantly strengthened by confinement. This is especially striking in a highly fissured rock, can be imagined as a mosaic of perfectly matching pieces. Sliding along the fissures is possible if the rock is free to displace normal to the average surface of rupture, as shown in Figure 3.8. But under confinement, the normal displacement required to move along such a jagged rupture path requires additional energy input. Thus it is not uncommon for a fissured rock to achieve an increase in strength by 10 times the amount of

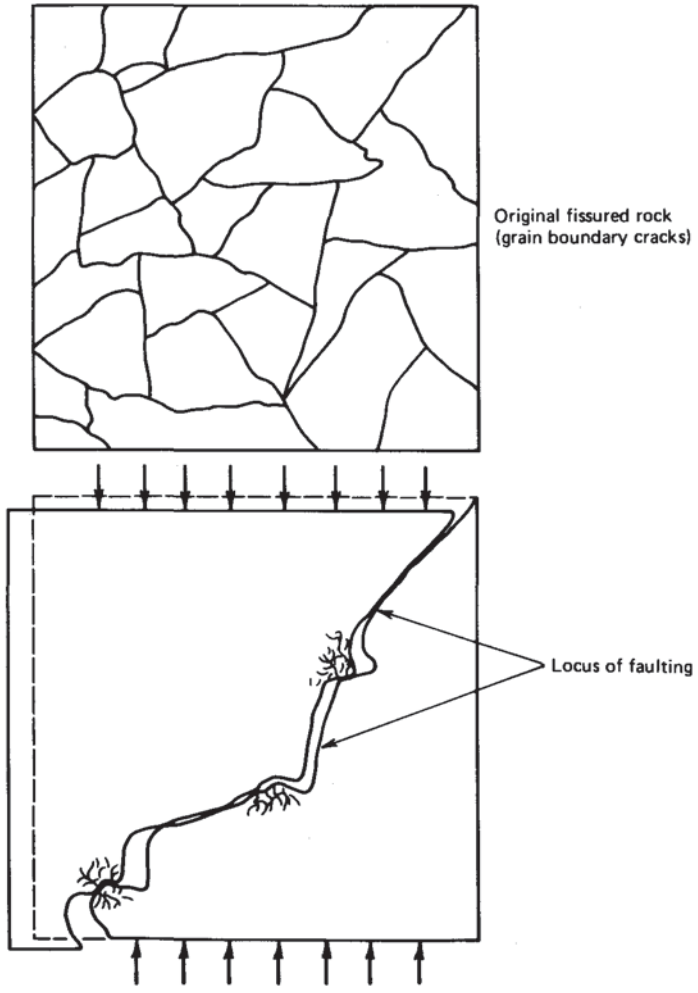

Figure 3.8 Dilatancy caused by roughness of the rupture surface.

a small increment in mean stress. This is one reason why rock bolts are so effective in strengthening tunnels in weathered rocks.

As mean pressure is increased, the rapid decline in load carrying capacity after the peak load (point D in Figure 3.7) becomes gradually less striking until, at a value of the mean pressure known as the *brittle-to-ductile transition pressure*, the rock behaves fully plastically (Figure 3.9). That is, after point D continued deformation of the rock is possible without any decrease in stress.

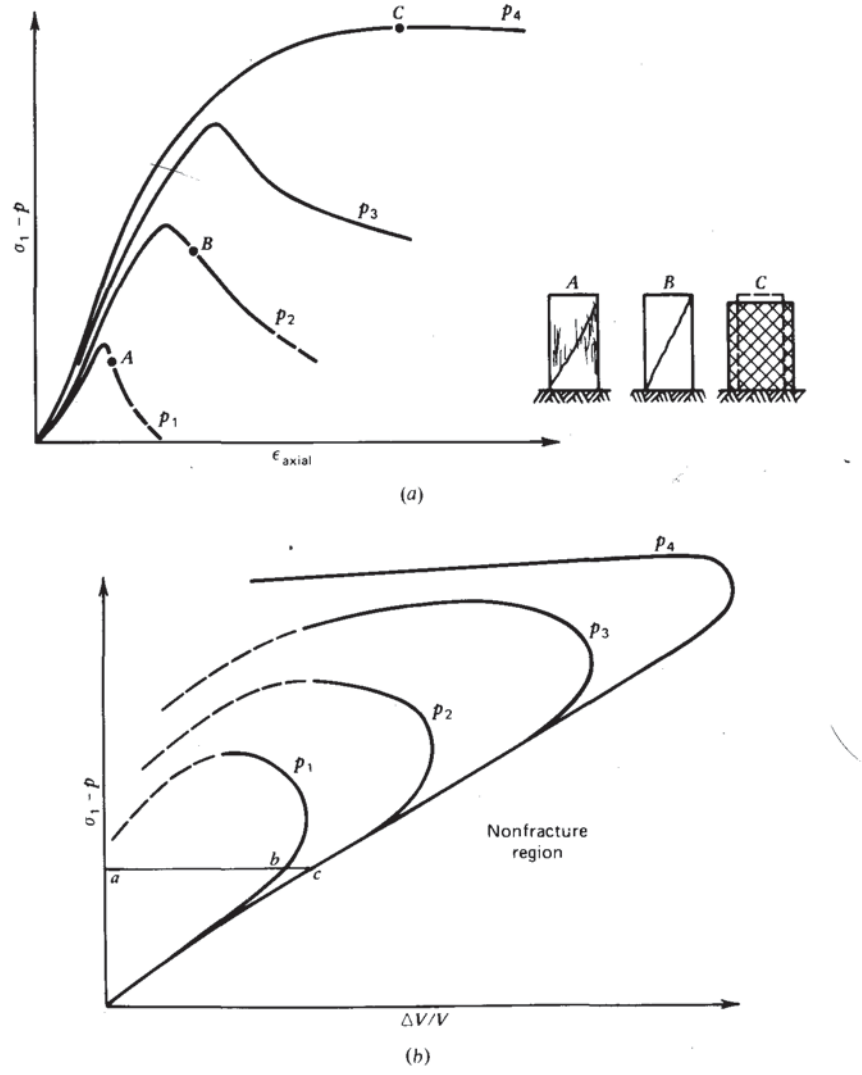

Figure 3.9 Behavior in triaxial compression. (*a*) Transition from brittle-to-ductile behavior. (*b*) Volumetric compression and dilatancy.

("Stress-hardening" behavior is sometimes observed at even higher pressures, meaning that there is actually a strengthening of the rock as it deforms without any "peak stress.") Figure 3.10 shows triaxial test data for a crystalline rock (norite) and a clastic rock (sandstone), both of which demonstrate loss of brittleness with confining pressure.

The brittle-to-ductile transition occurs at pressures far beyond the region of interest in most civil engineering applications. However, in evaporite rocks and soft clay shales, plastic behavior can be exhibited at engineering service loads. Table 3.2 lists some values of the transition pressure. Without confining pressure, most rocks tested past point *D* of Figure 3.7 will form one or more fractures parallel to the axis of loading (Figure 3.9*a*). When the ends are not smooth, the rock will sometimes split neatly in two, parallel to the axis, like a Brazilian specimen. As the confining pressure is raised, the failed specimen demonstrates faulting, with an inclined surface of rupture traversing the entire specimen. In soft rocks, this may occur even with unconfined specimens. If the specimen is too short, continued deformation past the faulting region will drive the edges of the fault blocks into the testing machine platens, producing complex fracturing in these regions and possibly apparent strain-hardening behavior. At pressures above the brittle-to-ductile transition, there is no failure per se, but the deformed specimen is found to contain parallel inclined lines that are the loci of intersection of inclined rupture surfaces and the surfaces of the specimen. Examination of the deformed rock will show intracrystalline twin gliding, intercrystal slip, and rupture.

The effect of confining pressure is also expressed in changing volumetric strain response as shown for a series of triaxial compression tests in Figure 3.9*b*. At successively higher confining pressures, the volumetric strain curves shift smoothly upward and to the right. These curves are the algebraic sum of hydrostatic compression under increasing mean stress (e.g., distance *ac*) and dilatancy under increasing deviatoric stress (*cb*). The response shown in Figure 3.9*b* applies when the ratio of σ_3 to σ_1 is sufficiently small. When this ratio is

***Table 3.2** Brittle-to-Ductile Transition Pressures for Rocks (At Room Temperature)*

Rock Type	Gage Pressure (MPa)	Gage Pressure (psi)
Rock salt	0	0
Chalk	<10	<1500
Compaction shale	0–20	0–3000
Limestone	20–100	3000–15,000
Sandstone	>100	>15,000
Granite	⩾100	⩾15,000

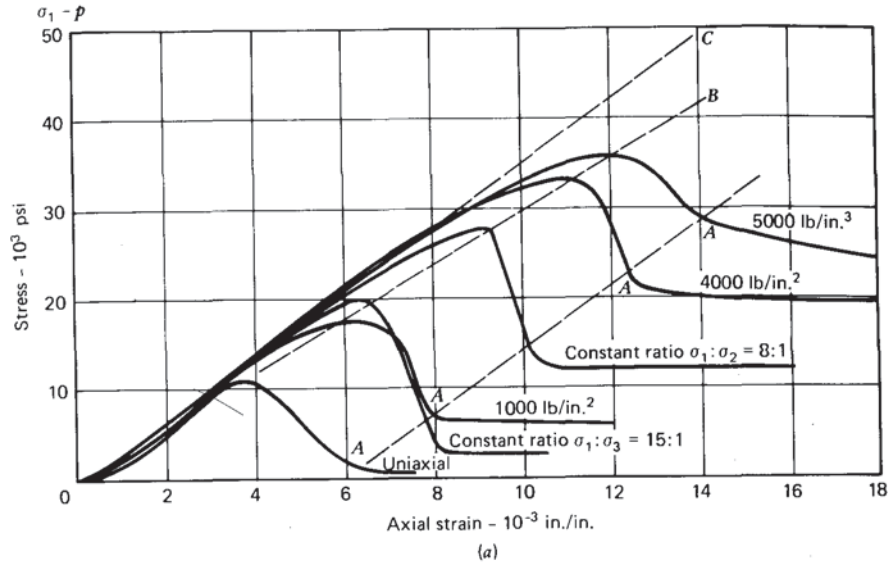

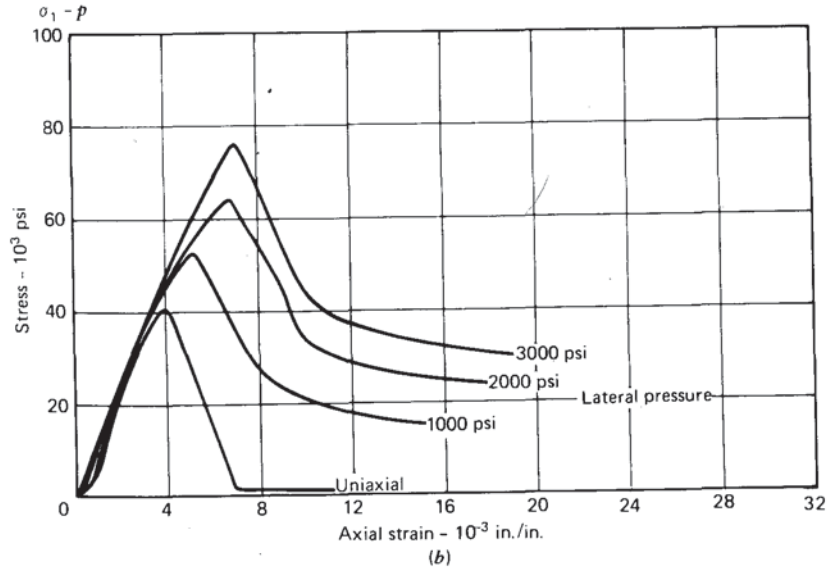

Figure 3.10 Stress difference versus axial strain curves as a function of confining pressure in triaxial compression experiments on sandstone (*a*) and norite (*b*). [From Bieniawski (1972).]

larger than a value of the order of 0.2, fracture does not occur and dilatancy is suppressed (as discussed in Section 3.8). In the usual triaxial test procedure, the principal stress ratio is decreased progressively during application of the deviator stress, until fracture occurs. But in practice, loading may occur such that the principal stress ratio remains fixed or increases.

3.4 The Meaning of "Rock Strength"

The word "failure" connotes an almost total loss of integrity in a sample of rock; in an engineering context, it usually implies loss of ability to perform the intended function. Obviously phenomena that constitute failure will depend on the function—varying from loss of a commodity in storage to structural collapse, property damage, and death. Even in a single specimen of rock, however, the concept of "failure" is unclear, for a total loss of cohesion occurs or does not occur in a single given rock according to the way it is loaded. The reason for such apparently fickle response is that the destruction of a rock by load is partly dependent on the loading system and is not a true rock property. For purposes of engineering design, it is useful to map *peak stress* values (i.e., the stresses corresponding to point D of Figure 3.7), and the criteria of failure discussed later will relate to such points. However, the compression test does not have to end in rupture at that point, but may proceed all the way to point E or beyond if the loading system is very stiff. The rock will exhibit what has been called "a complete stress-strain curve" if tested in a stiff system because the system responds to gradual deterioration in load-carrying capacity through automatic reduction in the applied load.

A testing machine is a reaction frame in which a screw or a hydraulic cylinder is operated to load a specimen. A screw-powered machine is characterized in Figure 3.11*a*. The rock specimen is fitted between a test table and an upper platen that are connected by stiff screws parallel to the axis of the specimen. A motor below the table turns a gear that causes the screws to turn thus bringing the upper platen up or down. If the screws are turned so that the rock specimen feels a load and then the motor is switched off, any subsequent movement of the upper platen relative to the table must alter the load at a rate given by the stiffness of the testing machine k_m. The family of lines marked A through J in Figure 3.11*b* describes the machine stiffness at different platen positions. Operation of the testing machine to build up load on a specimen corresponds to moving across the family of curves as shown in the figure. At the point of peak load of the rock, assuming we turn the motor off, the specimen will fail or not depending upon the relative values of k_r and k_m where k_r is the slope of the post peak portion of the complete stress-strain curve. For example, rock 1, Figure 3.11*b*, will continue to deform without sudden rupture as the testing machine is continuously shortened, whereas even with the machine turned off, rock 2 will fail because the machine as it "unstretches" cannot reduce the load sufficiently to satisfy the unloading requirements of the rock. However, if the motor were quickly switched to run backward and the upper platen were moved upward, it would be possible to follow the complete stress-strain curve of rock 2 as the system returned to curves G, F, etc. In a

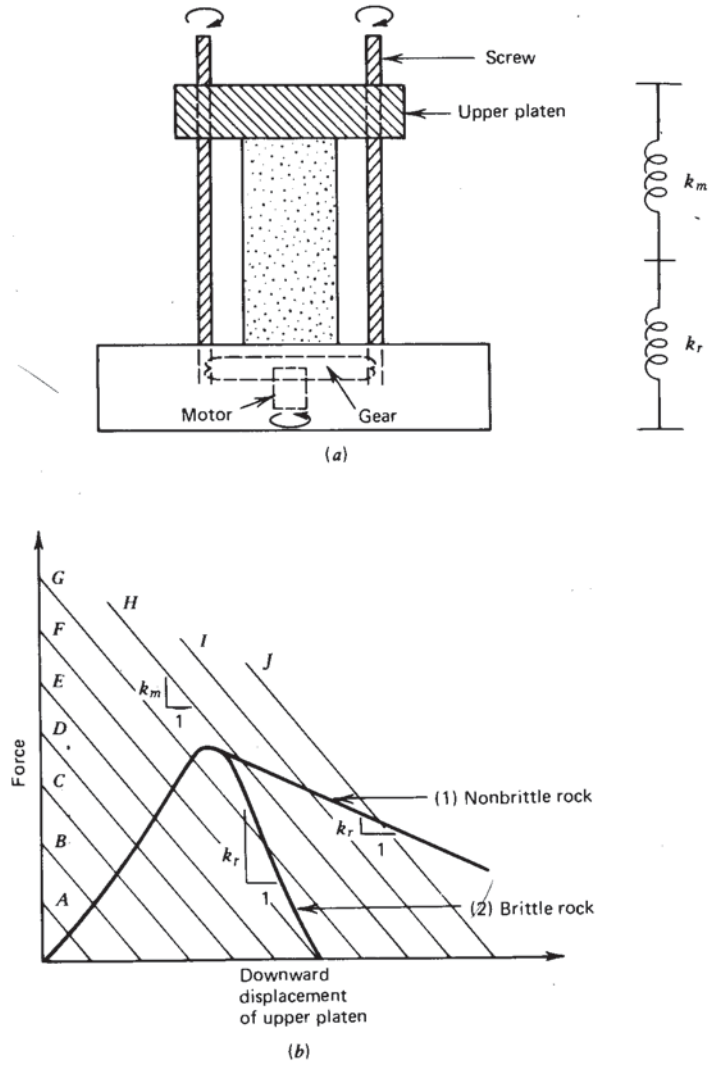

Figure 3.11 Influence of testing machine stiffness on failure. (*a*) A testing machine and its representation by a freebody. (*b*) Stable and unstable samples.

servocontrolled testing machine, this can be done automatically, the motor responding to the commands of an electrical circuit processing the signal of a deformation transducer attached to the specimen. Even without such a machine, it is possible to determine the complete stress-strain curve of a brittle rock by quick manual response, switching back and forth from loading to unloading modes. Figure 3.12 shows an actual record from such an operation with a specimen of coarse-grained marble (Chino marble, California). When the rock was loaded in the usual way in a 160,000-lb-capacity screw testing machine, the peak load was followed by a violent rupture that reduced the specimen to rock powder. By quickly unloading whenever the x-y plotter record revealed the onset of yielding, a series of hysteresis loops was created, the envelope to which estimates the right side of the complete stress-strain curve. At the end of the test, the specimen displayed a continuous fault but was still integral. Since the stiffness of the rock is proportional to its cross-sectional area, such a test is relatively easier to perform using small specimens. A convincing demonstration of the influence of the loading system stiffness on the mode of failure can be achieved by running two tests with varying machine stiffness while the rock stiffness is held constant. This can be achieved by adding a spring in series with the rock for one of the two tests.

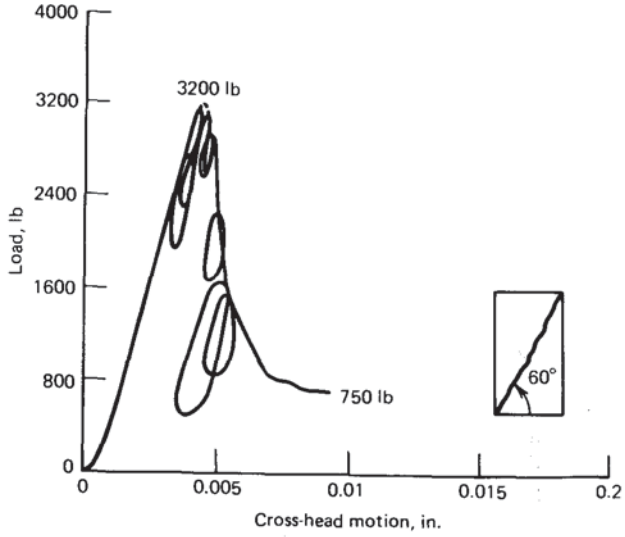

Figure 3.12 A complete stress-strain curve obtained by load cycling on a moderately stiff testing machine. The specimen was a coarse marble cylinder, 0.8 in. in diameter and 1.45 in. long.

3.5 Applications of the Complete Stress-Strain Curve

Normally when stresses become high enough to cause fractures in the wall of a tunnel or mine, rock simply spalls off, producing a destressed zone that drives the flow of stress away from the opening.

In a well-designed mine, the roof load will find somewhere else to go when a pillar collapses. But if a room and pillar mine were made with very wide rooms, the loss of one pillar might be insufferable.

These varying behavior modes in practice are understandable in terms of the complete stress-strain curve concept. In the mine with very wide rooms, the deflection of the roof due to the removal of one pillar can be calculated by assuming the roof span to be two rooms and one pillar wide. Using beam formulas or numerical model methods, the ratio of peak pillar load to the increment of roof deflection caused by removal of the pillar defines the *system stiffness*. If this stiffness is greater in magnitude than the slope of the postpeak part of the complete force-displacement curve, the mine can survive the failure of a pillar.

The complete stress-strain curve can also be used to preduct failure of rock as a result of *creep*. As shown in Figure 3.13, the locus of a creep test in the stress-strain graph is a horizontal line. If the initial stress in the rock is close to the peak load, creep will terminate in rupture when accumulated strain is such as to intersect the falling part of the complete stress-strain curve. A creep test started at A will terminate in rupture at point B after a relatively short time. A

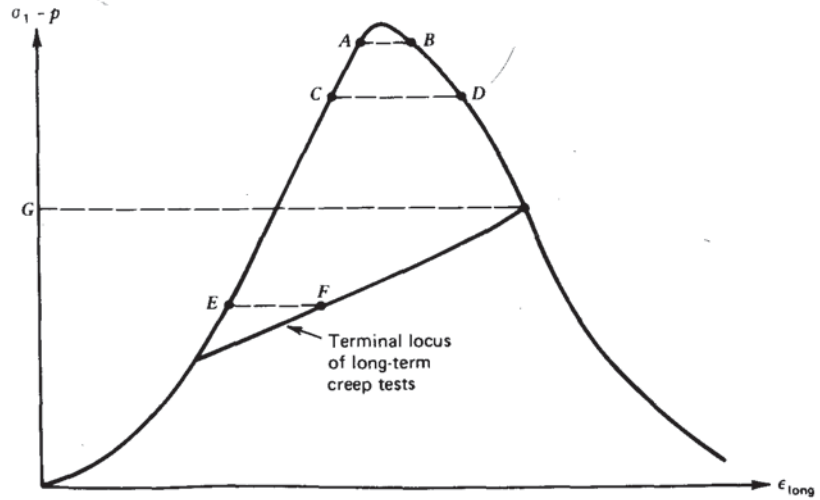

Figure 3.13 Creep in relation to the complete stress-strain curve.

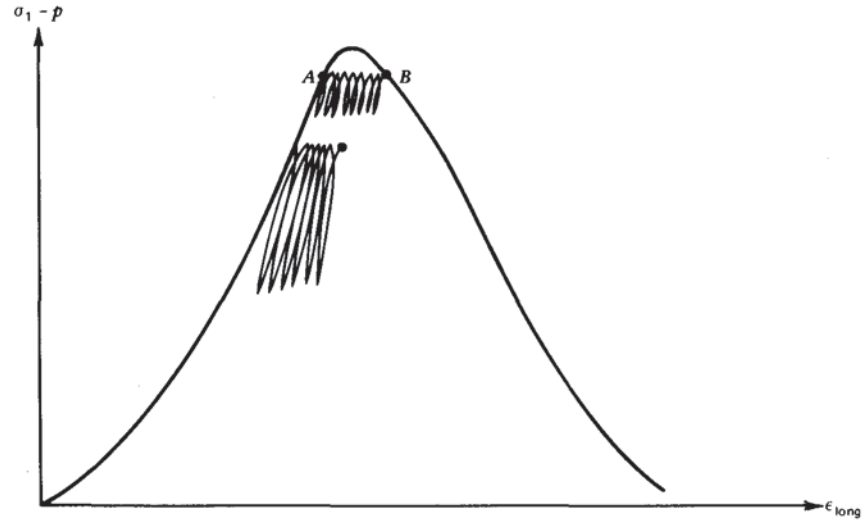

Figure 3.14 Response to dynamic loading, in relation to the complete stress-strain curve.

creep test begun at C will terminate in rupture at D after a much longer time. And a creep test initiated at E below critical stress level G will approach point F without rupture after a long time (compare with Figure 6.16).

A similar concept applies to *cyclic loading* beneath the peak load level, as shown in Figure 3.14. Cycles of loading and unloading produce "hysteresis loops" as energy is consumed in sliding on cracks and fissures inside the rock volume. Multiple load cycles begun at point A such that the peak load is never surpassed will cause a migration of the envelope of hysteresis loops which terminate in rupture at point B.[3]

3.6 The Mohr-Coulomb Failure Criterion

We have noted that the peak stress of rock undergoing deviatoric loading will increase if the rock is confined. The variation of peak stress σ_1 with confining pressure σ_3 is known as a *criterion of failure*. The simplest and best-known criterion of failure for rocks is the Mohr-Coulomb criterion; as shown in Figure 3.15, this consists of a linear envelope touching all Mohr's circles representing

[3] This suggests a method of relieving stored energy along faults near the rupture point by cyclic loading. Professor B. Haimson of the University of Wisconsin proposed this be done by cyclic pumping of water from wells in the fault zone. The effect of water pressure is considered in Section 3.7.

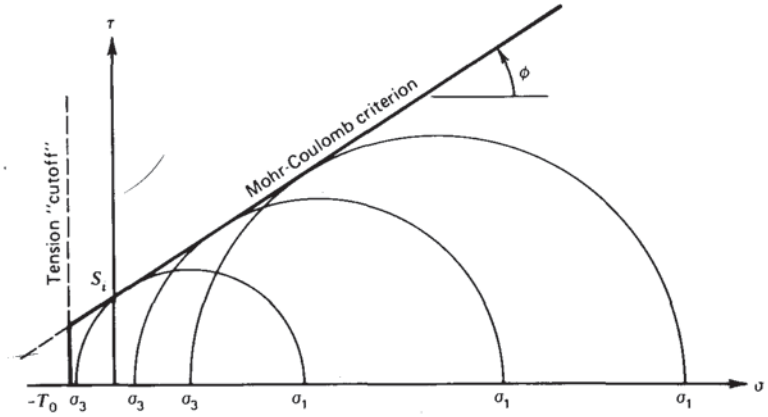

Figure 3.15 The Mohr-Coulomb failure criterion with a tension cutoff.

critical combinations of principal stresses. Stated in terms of normal and shear stresses on the plane represented by the point of tangency of a Mohr circle with the envelope

$$\tau_p = S_i + \sigma \tan \phi \tag{3.7}$$

ϕ is called the angle of internal friction, for like a friction angle for sliding between surfaces, it describes the rate of increase of peak strength with normal stress. τ_p is the peak shear stress, or *shear strength*.

The Mohr-Coulomb criterion is also used to represent the "residual" strength, that is, the minimum strength reached by a material subjected to deformation beyond the peak, as shown in Figure 3.10. In this case, the subscript r may be used with each of the terms of Equation 3.7 to identify them as parameters of residual strength. The residual shear strength ($S_{i,r}$ may approach zero while the residual friction angle ϕ_r will usually lie between zero and the peak friction angle. However, in compaction shales rich in montmorillonite, like the Cretaceous Bearpaw and Pierre shales, values as low as 4–6° are reported, even in "drained" test arrangements that prevent pore water pressure accumulation during deformation (Townsend and Gilbert, 1974).

Equation 3.7 has the following physical interpretation. "Failure" occurs when the applied shear stress less the frictional resistance associated with the normal stress on the failure plane becomes equal to a constant of the rock, S_i. Since it would not be reasonable to admit a frictional resistance in the presence of a tensile normal stress, this equation then loses its physical validity when the value of σ crosses into the tensile region; σ represents the normal stress on the plane of failure. The minimum principal stress σ_3 may be tensile as long as σ remains compressive. Other theories of failure (e.g., the Griffith theory) are

more exact in the tensile region. However, the Mohr-Coulomb theory has the merit of simplicity and will be retained here by extrapolating the Mohr-Coulomb line into the tensile region up to the point where σ_3 becomes equal to the uniaxial tensile strength $-T_0$. The minor principal stress can never be less than $-T_0$.

Respecting the last as a constraint on the criterion of failure is, in effect, recognizing a "tension cutoff" superimposed on the Mohr-Coulomb criterion of failure as shown in Figure 3.15. The actual envelope of critical Mohr's circles with one principal stress negative will lie beneath the Mohr-Coulomb criterion with the superimposed tension cutoff as indicated in Figure 3.16, so it is necessary to reduce the tensile strength T_0 and the shear strength intercept S_i when applying this simplified failure criterion in any practical situation.

In terms of the principal stresses at peak load conditions, the Mohr-Coulomb criterion can be written

$$\sigma_{1,p} = q_u + \sigma_3 \tan^2\left(45 + \frac{\phi}{2}\right) \tag{3.8}$$

where $\sigma_{1,p}$ is the major principal stress corresponding to the peak of the stress-strain curve, and q_u is the unconfined compressive strength. The change of variables leads to the following relationship between shear strength intercept S_i and unconfined compressive strength q_u

$$q_u = 2S_i \tan\left(45 + \frac{\phi}{2}\right) \tag{3.9}$$

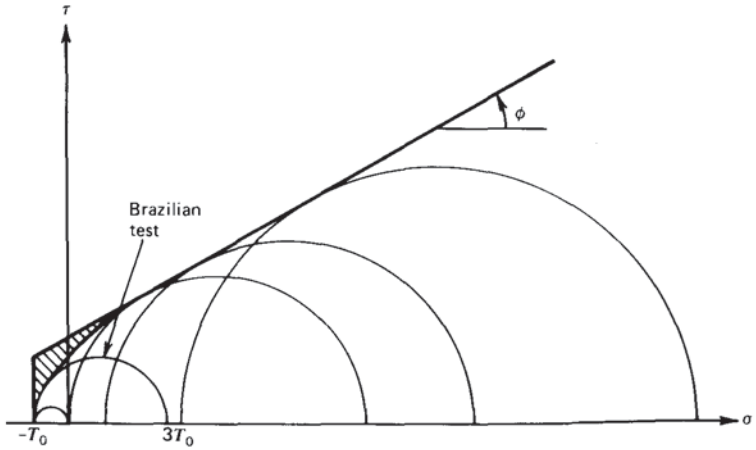

Figure 3.16 Comparison of empirical envelope and Mohr-Coulomb criterion in the tensile region. Inside the ruled region, the Mohr-Coulomb criterion with tension cutoff overestimates the strength.

Table 3.3 *Representative Values for Shear Strength Intercept (S_i) and Angle of Internal Friction (ϕ) for Selected Rocks*[a]

Description	Porosity (%)	S_i (MPa)	ϕ	Range of Confining Pressure (MPa)	Reference[b]
Berea sandstone	18.2	27.2	27.8	0–200	4
Bartlesville sandstone		8.0	37.2	0–203	3
Pottsville sandstone	14.0	14.9	45.2	0–68.9	8
Repetto siltstone	5.6	34.7	32.1	0–200	4
Muddy shale	4.7	38.4	14.4	0–200	4
Stockton shale		0.34	22.0	0.8–4.1	2
Edmonton bentonitic shale (water content 30%)	44.0	0.3	7.5	0.1–3.1	9
Sioux quartzite		70.6	48.0	0–203	3
Texas slate; loaded					
30° to cleavage		26.2	21.0	34.5–276	6
90° to cleavage		70.3	26.9	34.5–276	6
Georgia marble	0.3	21.2	25.3	5.6–68.9	8
Wolf Camp limestone		23.6	34.8	0–203	3
Indiana limestone	19.4	6.72	42.0	0–9.6	8
Hasmark dolomite	3.5	22.8	35.5	0.8–5.9	4
Chalk	40.0	0	31.5	10–90	1
Blaine anhydrite		43.4	29.4	0–203	3
Inada biotite granite	0.4	55.2	47.7	0.1–98	7
Stone Mountain granite	0.2	55.1	51.0	0–68.9	8
Nevada Test Site basalt	4.6	66.2	31.0	3.4–34.5	10
Schistose gneiss					
90° to schistocity	0.5	46.9	28.0	0–69	2
30° to schistocity	1.9	14.8	27.6	0–69	2

[a] Data from Kulhawy (1975) (Ref. 5).

[b]

1. Dayre, M., Dessene, J. L., and Wack, B. (1970) *Proc. 2nd Congress of ISRM*, Belgrade, Vol. 1, pp. 373–381.
2. DeKlotz, E., Heck, W. J., and Neff, T. L. (1964) First Interim Report, *MRD Lab Report 64/493*, U. S. Army Corps of Engineers, Missouri River Division.
3. Handin, J. and Hager, R. V. (1957) *Bull. A.A.P.G.* **41:** 1–50.
4. Handin, J., Hager, R. V., Friedman, M., and Feather, J. N. (1963) *Bull. A.A.P.G.* **47:** 717–755.
5. Kulhawy, F. (1975) *Eng. Geol.* **9:** 327–350.
6. McLamore, R. T. (1966) Strength-deformation characteristics of anisotropic sedimentary rocks, Ph.D. Thesis, University of Texas, Austin.
7. Mogi, K. (1964) *Bull. Earthquake Res. Inst.*, Tokyo, Vol. 42, Part 3, pp. 491–514.
8. Schwartz, A. E. (1964) *Proc. 6th Symp. on Rock Mech.*, Rolla, Missouri, pp. 109–151.
9. Sinclair, S. R. and Brooker, E. W. (1967) *Proc. Geotech. Conf. on Shear Strength Properties of Natural Soils and Rocks*, Oslo, Vol. 1, pp. 295–299.
10. Stowe, R. L. (1969) U. S. Army Corps of Engineers Waterways Experiment Station. Vicksburg, *Misc. Paper C-69-1*.

The maximum tension criterion must be superimposed on Equation 3.8, that is, failure is presumed to occur because of tensile stress whenever σ_3 becomes equal to $-T_0$, regardless of the value of σ_1.

Typical values of the peak shear strength intercept S_i and the peak angle of internal friction ϕ for a representative set of rock specimens are listed in Table 3.3. The ratio of unconfined compressive to tensile strength a_u/T_0 for a sampling of rock types is given in Table 3.1.

3.7 The Effect of Water

Some rocks are weakened by the addition of water, the effect being a chemical deterioration of the cement or clay binder. A friable sandstone may, typically, lose 15% of its strength by mere saturation. In extreme cases, such as montmorillonitic clay shales, saturation is totally destructive. In most cases, however, it is the effect of pore and fissure water pressure that exerts the greatest influence on rock strength. If drainage is impeded during loading, the pores or fissures will compress the contained water, raising its pressure.

Development of pore pressure and consequent loss in strength of a Pennsylvanian shale tested in triaxial compression is shown in Figure 3.17. Two separate test results are presented in this diagram: the circles represent triaxial compression of a saturated specimen under conditions such that excess pore pressures could drain away rather than accumulate ("drained conditions"); the triangles represent a saturated shale specimen tested without drainage, so that excess pore pressures that develop must accumulate ("undrained conditions"). The curve of differential axial stress versus axial strain for the drained test displays a peak and then a descending tail as depicted in Figure 3.7*a*. Since the mean stress increases simultaneously with the axial stress in a triaxial test, the curve of volumetric strain shown in Figure 3.17 is the sum of hydrostatic compression (Figure 3.6) and dilatancy behavior (Figure 3.7*b*). Initially, the volume decreases by hydrostatic compression until the specimen begins to dilate, whereupon the rate of volume decrease slows, eventually becoming negative, meaning the volume increases on subsequent load increments. In the undrained test, the tendency for volume change cannot be fully realized because the water filling the voids undergoes compression rather than drainage. As a result, the water pressure p_w inside the pores begins to increase. This dramatically lowers the peak stress and flattens the postpeak curve.

Many investigators have confirmed the validity of Terzaghi's *effective stress law* for rocks, which states that a pressure of p_w in the pore water of a rock will cause the same reduction in peak normal stress as caused by a reduction of the confining pressure by an amount equal to p_w. We can make use of this result by introducing the term *effective stress* σ' defined by

$$\sigma' = \sigma - p_w \tag{3.10}$$

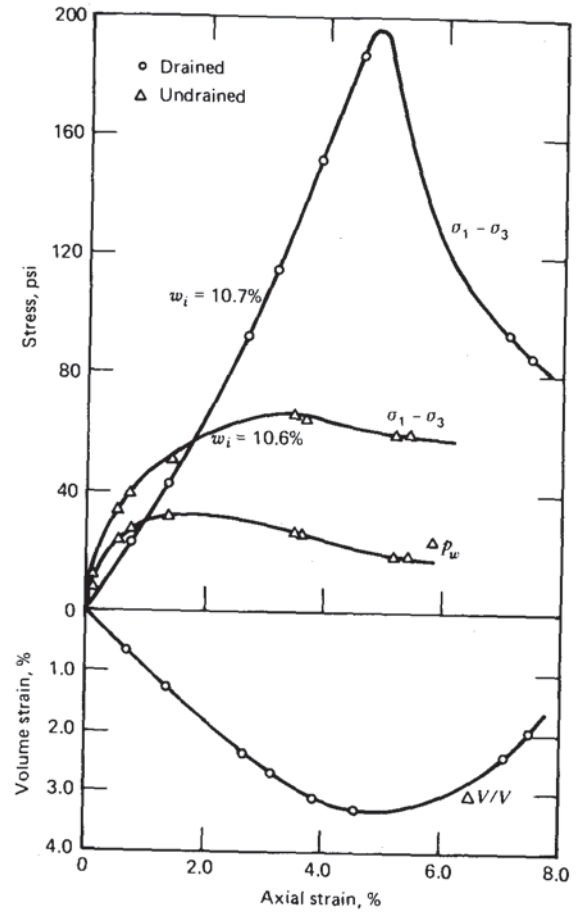

Figure 3.17 Drained and undrained triaxial compression test results for a shale of Pennsylvanian age; w_i is the initial water content; p_w is the pore water pressure. (From Mesri and Gibala, 1972.)

Differential stress $(\sigma_1 - \sigma_3)$ is unaffected by water pressure since $\sigma_1' - \sigma_3' = (\sigma_1 - p_w) - (\sigma_3 - p_w) = \sigma_1 - \sigma_3$.

The effect of water pressure can be input in the failure criterion simply by restating the conditions for failure in terms of effective stresses. In a test on a dry rock, there is no difference between normal stresses and effective normal stresses. For a saturated rock, rewrite Equation 3.8 in terms of effective stress by introducing $'$ on the normal stress terms:

$$\sigma_{1,p}' = q_u + \sigma_3' \tan^2\left(45 + \frac{\phi}{2}\right) \tag{3.11}$$

or

$$\sigma_{1,p}' - \sigma_3' = q_u + \sigma_3' \left[\tan^2\left(45 + \frac{\phi}{2}\right) - 1\right] \tag{3.12}$$

Since the differential stress is unaffected by pore pressure, Equation 3.12 may also be written

$$\sigma_{1,p} - \sigma_3 = q_u + (\sigma_3 - p_w) \left[\tan^2\left(45 + \frac{\phi}{2}\right) - 1\right]$$

Solving for p_w, we can calculate the water pressure in the pores or fissures of a rock required to initiate failure from an initial state of stress defined by σ_1 and σ_3:

$$p_w = \sigma_3 - \frac{(\sigma_1 - \sigma_3) - q_u}{\tan^2(45 + \phi/2) - 1} \tag{3.13}$$

Figure 3.18 portrays this condition graphically. The buildup of water pressure in the rock near a reservoir or in an aquifer can cause rock failure and earthquakes, if the rock is initially stressed near the limit. However, earthquakes induced by reservoir construction and by pumping water into deep aquifers are believed to originate from rupture along preexisting faults in determined orientations. The mechanism is similar but the equations contain the influence of the relative directions of initial stress as discussed in Chapter 5 (compare with Equation 5.9).

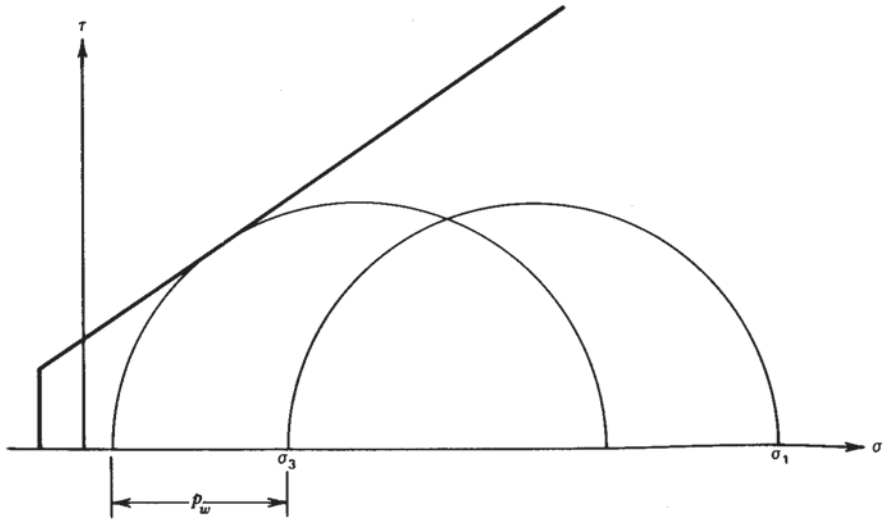

Figure 3.18 Water pressure required to initiate failure of an intact rock from a given initial state of stress.

3.8 The Influence of the Principal Stress Ratio on Failure

In the usual triaxial compression experiment, the rock is seated with a hydrostatic stress, that is, with a principal stress ratio $K = \sigma_3/\sigma_1$ equal to unity. Thereafter, as σ_1 is raised, the value of K is reduced until cracking occurs, and eventually peak strength is reached. This may not be a realistic loading path for all situations, and it may be desirable to consider rock behavior when the principal stress ratio is fixed at some value. In examining the conditions resulting from excavating an underground chamber in a rock mass, for example, the directions and relative magnitudes of principal stresses can be found throughout the region of influence of the opening. Changing the assumption about the magnitudes of the initial stresses will increase or decrease these stresses but will not alter any value of K as long as the rock behaves elastically. Therefore, there is some merit in expressing the criterion of failure in terms of the principal stress ratio, as discussed by Hoek (1968). When this is done, it is easily seen that there is a value of K above which failure cannot occur, and this can be verified by tests. In terms of the Mohr-Coulomb criterion of failure, dividing both sides of Equation 3.8 by $\sigma_{1,P}$ and introducing $K = \sigma_3/\sigma_1$ yields

$$\sigma_{1,p} = \frac{q_u}{1 - K\tan^2(45 + \phi/2)} \tag{3.14}$$

from which we can see that the peak major principal stress becomes large when K approaches $\cot^2(45 + \phi/2)$. For example, for $\phi = 45°$, failure cannot occur above a principal stress ratio $K = 0.17$.

3.9 Empirical Criteria of Failure

While the Mohr-Coulomb criterion is easy to work with and affords a useful formula for manipulation in practical situations, a more precise criterion of failure can be determined for any rock by fitting an envelope to Mohr's circles representing values of the principal stresses at peak conditions in laboratory tests. As shown in Figure 3.19, this envelope will frequently curve downward. Jaeger and Cook (1976)[4] and Hoek (1968) demonstrated that the failure envelopes for most rocks lie between a straight line and a parabola. The Griffith theory of failure predicts a parabola in the tensile stress region. This theory is premised on the presence of randomly oriented fissures in the rock that act to create local stress concentrations, facilitating new crack initiation. However, the Griffith theory has no physical basis in the region where both principal

[4] See references, Chapter 1.

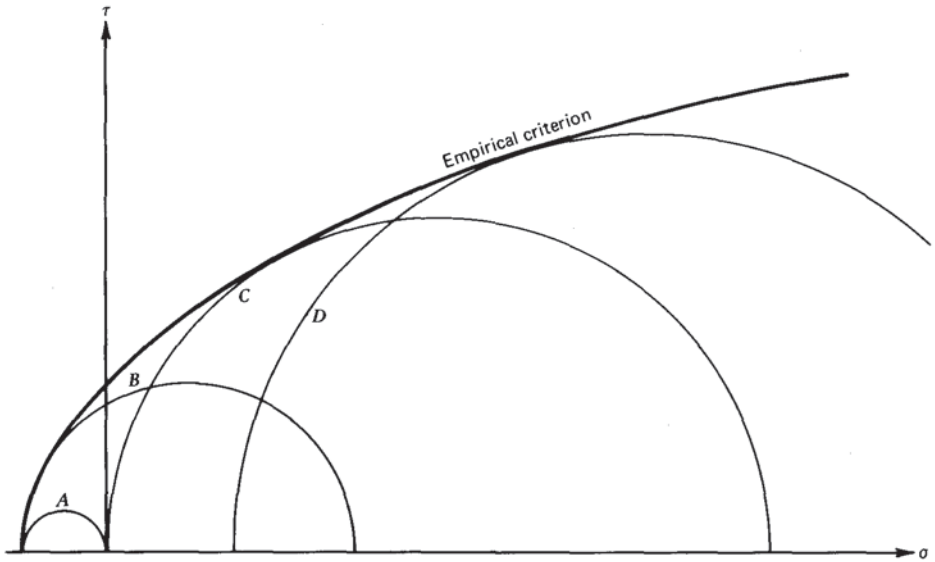

Figure 3.19 An empirical criterion of failure defined by the envelope to a series of Mohr's circles: *A*, direct tension; *B*, Brazilian; *C*, unconfined compression; *D*, triaxial compression.

stresses are compressive. In practice, empirical curve fitting is the best procedure for producing a criterion of failure tailored to any given rock type. See, for example, Herget and Unrug (1976). A satisfactory formula for many purposes will be afforded by the union of a tension cutoff, $\sigma_3 = -T_0$, and a power law (Bieniawski, 1974):

$$\frac{\sigma_{1,p}}{q_u} = 1 + N\left(\frac{\sigma_3}{q_u}\right)^M \tag{3.15}$$

The constants N and M will be determined by fitting a curve to the family of points

$$\left(\frac{\sigma_3}{q_u}, \frac{\sigma_{1,p}}{q_u} - 1\right)$$

Another approach fits data from the ring shear test (Figure 3.3*e*) to find an empirical equation for a Mohr envelope of intact rock (Lundborg, 1966). The peak shear strength (τ_p) (Equation 3.4) is plotted against σ to define the strength envelope, Figure 3.20*a*. Lundborg found that such data define a curved envelope with intercept S_i and asymptote S_f, fit by

$$\tau_p = S_i + \frac{\mu'\sigma}{1 + \dfrac{\mu'\sigma}{S_f - S_i}} \tag{3.16}$$

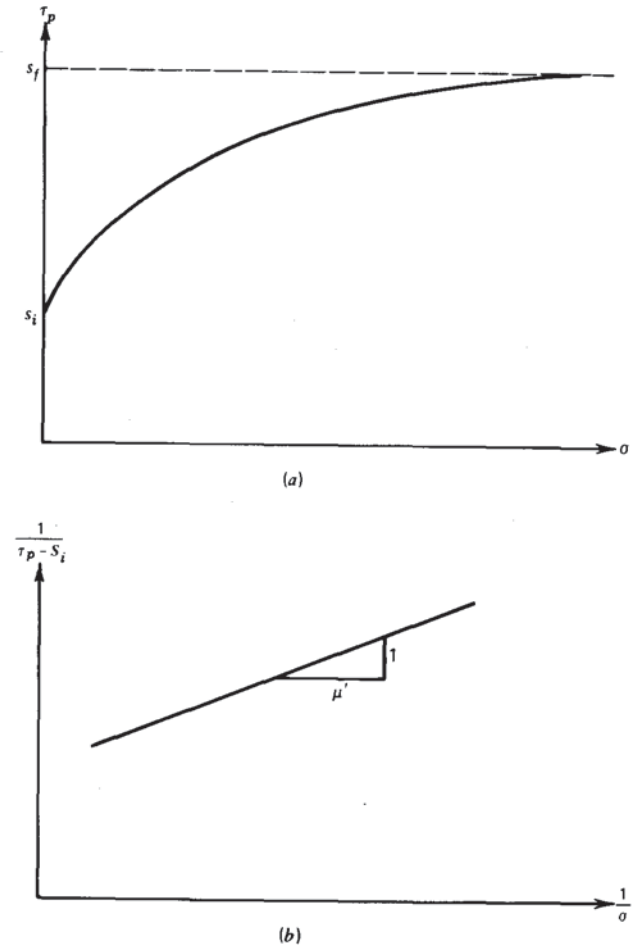

Figure 3.20 An empirical criterion of failure derived from the ring shear test. (After Lundborg, 1966.) (a) A plot of equation 3.16; (b) graphical determination of μ'.

(The symbol μ' has been used in place of Lundborg's μ to distinguish this coefficient from the Mohr-Coulomb coefficient of internal friction, $\mu = \tan\phi$.) Equation 3.16 can also be written

$$\frac{1}{\tau_p - S_i} = \frac{1}{\mu'\sigma} + \frac{1}{S_f - S_i} \tag{3.17}$$

so that μ' is determined as the inverse of the slope of the line obtained by plotting $(\tau_p - S_i)^{-1}$ as ordinate against $(\sigma)^{-1}$ as abscissa (Figure 3.20*b*). Table 3.4 lists typical values of Lundborg's parameters. Strengths determined by ring

Table 3.4 *Some Values of Constants for Lundborg's Strength Equation*

	μ'	S_i (MPa)	S_f (MPa)
Granite	2.0	60	970
Pegmatite	2.5	50	1170
Quartzite	2.0	60	610
Slate	1.8	30	570
Limestone	1.2	30	870

shear tend to be slightly higher than corresponding strengths determined by triaxial tests.

3.10 The Effect of Size on Strength

Rocks are composed of crystals and grains in a fabric that includes cracks and fissures; understandably, rather large samples are required to obtain statistically complete collections of all the components that influence strength. When the size of a specimen is so small that relatively few cracks are present, failure is forced to involve new crack growth, whereas a rock mass loaded through a larger volume in the field may present preexisting cracks in critical locations. Thus rock strength is size dependent. Coal, altered granitic rocks, shale, and other rocks with networks of fissures exhibit the greatest degree of size dependency, the ratio of field to laboratory strengths sometimes attaining values of 10 or more.

A few definitive studies have been made of size effect in compressive strength over a broad spectrum of specimen sizes. Bieniawski (1968) reported tests on prismatic in situ coal specimens up to 1.6 × 1.6 × 1 m, prepared by cutting coal from a pillar; the specimens were then capped with strong concrete and loaded by hydraulic jacks. Jahns (1966) reported results of similar tests on cubical specimens of calcareous iron ore; the specimens were prepared by means of slot cutting with overlapping drill holes. Jahns recommended a specimen size such that 10 discontinuities intersect any edge. Larger specimens are more expensive without bringing additional size reduction, while smaller specimens yield unnaturally high strengths. Available data are too sparse to accept Jahn's recommendation for all rock types but it does appear that there is generally a size such that larger specimens suffer no further decrease in

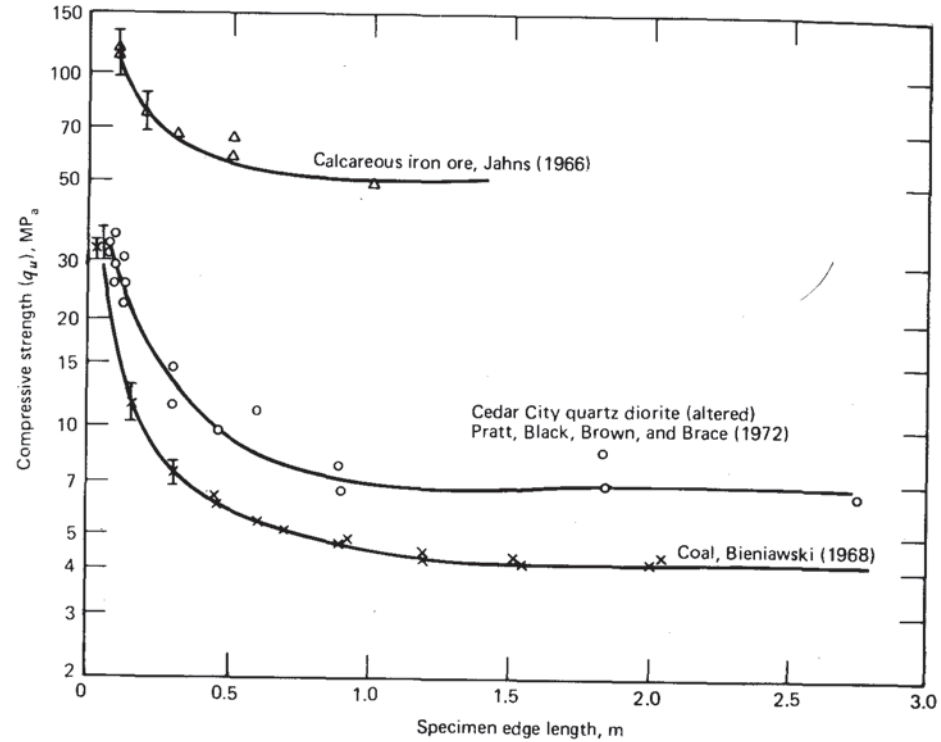

Figure 3.21 Effect of specimen size on unconfined compressive strength. (After Bieniawski and Van Heerden, 1975.)

strength. Figure 3.21 demonstrates this pattern of behavior in a summary of the tests on coal and iron ore, as well as tests on an altered and fissured quartz diorite by Pratt et al. (1972). This clever series of tests included specimens of equilateral triangular cross section 6 ft (1.83 m) on edge, and 9 ft (2.74 m) long, loaded via stainless steel flat jacks in a vertical slot at one end. Figure 3.22*a* shows a specimen being freed by drilling a slot inclined at 60° and Figure 3.22*b* shows the surface of the specimen, with completed slots, jacks in place on one end, and extensometers positioned for strain measurements on the surface. The quartz diorite tested displayed a large size effect because it contains highly fractured plagioclase and amphibole phenocrysts in a finer-grained ground mass with disseminated clay; the porosity of this rock is 8–10%.

The influence of size on shear and tension tests is less well documented but undoubtedly as severe for rocks that contain discontinuities. The subject of scale effect will be considered further in Chapter 7 in the context of underground openings.

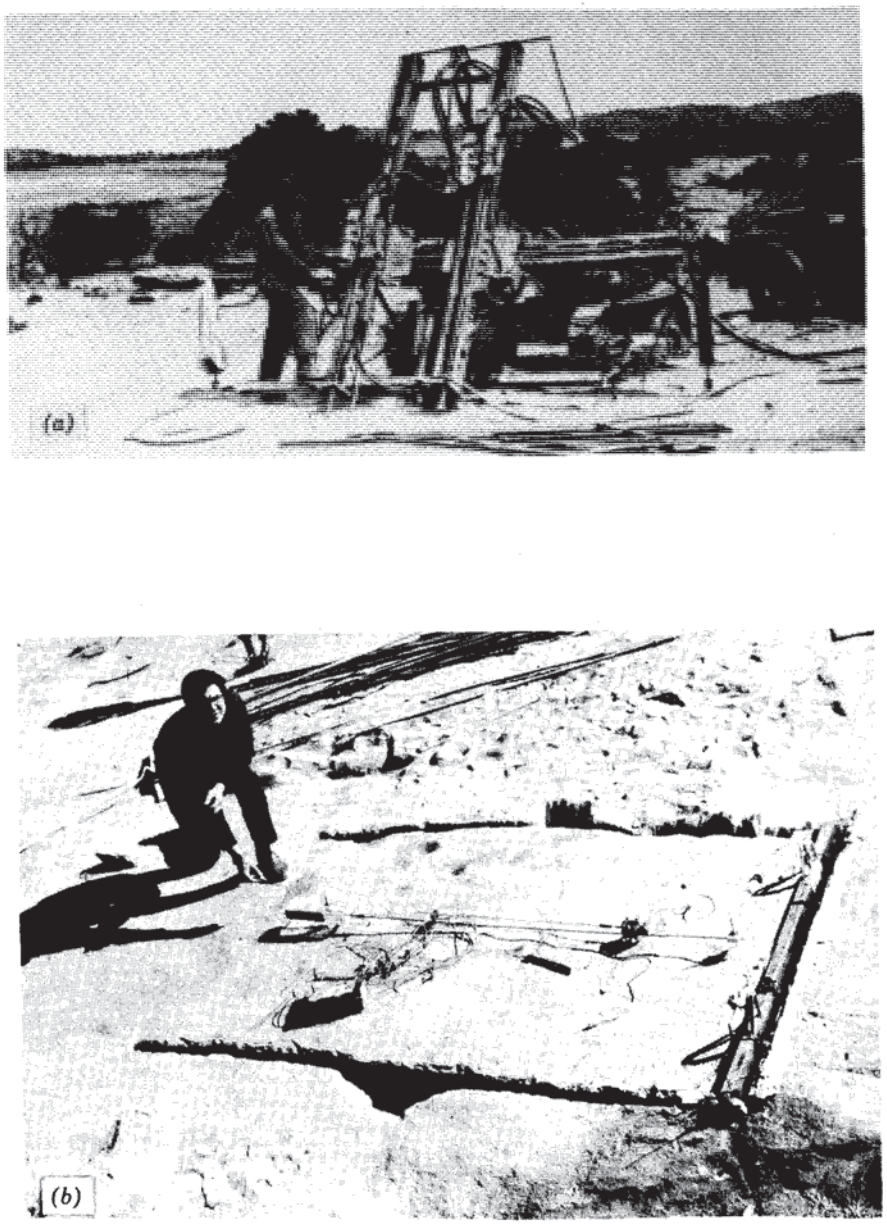

Figure 3.22 Large uniaxial compression tests conducted in-situ by TerraTek on Cedar City Quartz Diorite. (*a*) Drilling a line of 1–1/2-inch diameter holes plunging 60° to create an inclined slot forming one side of the triangular prism "specimen." (*b*) A view of the test site showing flat jacks at one end and extensometers for relative displacement measurement during loading. (Courtesy of H. Pratt.)

3.11 Anisotropic Rocks

Variation of compressive strength according to the direction of the principal stresses is termed "strength anisotropy." Strong anisotropy is characteristic of rocks composed of parallel arrangements of flat minerals like mica, chlorite, and clay, or long minerals like hornblende. Thus the metamorphic rocks, especially schist and slate, are often markedly directional in their behavior. For example, Donath (1964) found the ratio of minimum to maximum unconfined compressive strength of Martinsburg slate to be equal to 0.17. Anisotropy also occurs in regularly interlayered mixtures of different components, as in banded gneisses, sandstone/shale alternations, or chert/shale alternations. In all such rocks, strength varies continuously with direction and demonstrates pronounced minima when the planes of symmetry of the rock structure are oblique to the major principal stress.

Rock masses cut by sets of joints also display strength anisotropy, except where the joint planes lie within about 30° of being normal to the major principal stress direction. The theory of strength for jointed rocks is discussed in Chapter 5.

Strength anisotropy can be evaluated best by systematic laboratory testing of specimens drilled in different directions from an oriented block sample. Triaxial compression tests at a set of confining pressures for each given orientation then determine the parameters S_i and ϕ as functions of orientation. Expanding on a theory introduced by Jaeger (1960), McLamore (1966) proposed that both S_i and ϕ could be described as continuous functions of direction according to

$$S_i = S_1 - S_2[\cos 2(\psi - \psi_{\min,s})]^n \tag{3.18}$$

and

$$\tan \phi = T_1 - T_2[\cos 2(\psi - \psi_{\min,\phi})]^m \tag{3.19}$$

where S_1, S_2, T_1, T_2, m, and n are constants
ψ is the angle between the direction of the cleavage (or schistocity, bedding or symmetry plane) and the direction σ_1
$\psi_{\min,s}$ and $\psi_{\min,\phi}$ are the values of ψ corresponding to minima in S_i and ϕ, respectively

For a slate, McLamore determined that friction and shear strength intercept minima occur at different values of ψ, respectively 50 and 30°. The strength parameters for the slate are

$$S_i = 65.0 - 38.6[\cos 2(\psi - 30)]^3 \text{ (MPa)} \tag{3.18a}$$

and

$$\tan \phi = 0.600 - 0.280 \cos 2(\psi - 50) \tag{3.19a}$$

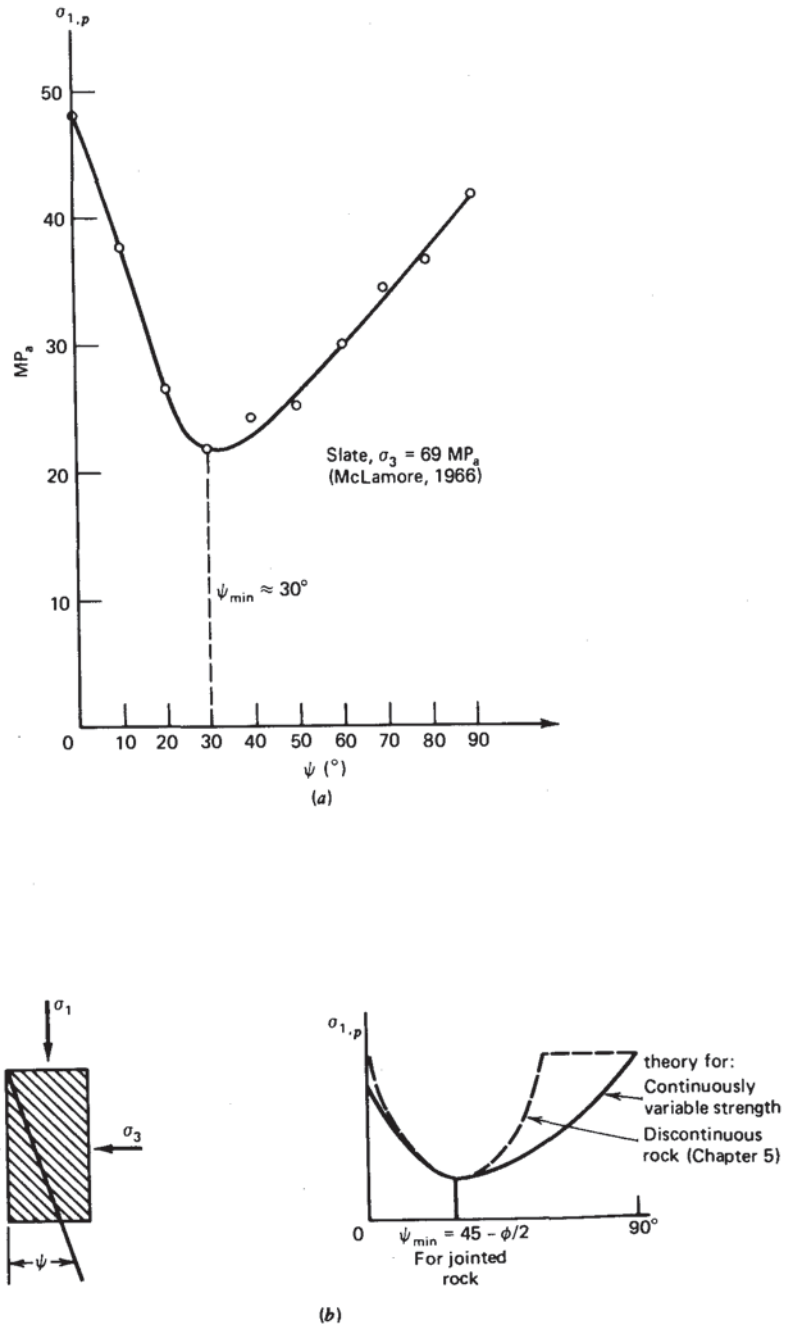

Figure 3.23 Strength anisotropy in triaxial compression.

In general, the entire range of ψ from 0 to 90° cannot be well fit with one set of constants since the theory (Equations 3.18 and 3.19) would then predict strength at $\psi = 0°$ to be less than the strength at $\psi = 90°$; in fact, the strength when loading is parallel to slaty cleavage, schistosity, or bedding is usually higher than the strength when the loading is perpendicular to the planes of weakness within the rock. (Compare Figures 3.23*a* and *b*.) For oil shale, a repetitive layering of marlstone and kerogen, McLamore used one set of constants for the region $0° \leq \psi < 30°$ and a second set of constants for $30° \leq \psi \leq 90°$.

The variation of the friction angle with direction proves generally less severe than the variation of the shear strength intercept. As a simplification, assume $n = 1$, $\psi_{min,s} = 30°$, and ϕ independent of direction ($m = 0$). Then the strength anisotropy can be evaluated from compressive tests run at $\psi = 30°$ and $\psi = 75°$ (see Problem 12).

References

Bieniawski, Z. T. (1967a) Stability concept of brittle fracture propagation in rock, *Eng. Geol.* **2:** 149–162.

Bieniawski, Z. T. (1967b) Mechanism of brittle fracture of rock, *Int. J. Rock Mech. Min. Sci.* **4:** 395–430.

Bieniawski, Z. T. (1968) The effect of specimen size on compressive strength of coal, *Int. J. Rock Mech. Min. Sci.* **5:** 325–335.

Bieniawski, Z. T. (1972) Propagation of brittle fracture in rock, *Proceedings, 10th Symposium on Rock Mechanics* (AIME), pp. 409–427.

Bieniawski, Z. T. (1974) Estimating the strength of rock materials, *J. South African Inst. Min. Metall.* **74:** 312–320.

Bieniawski, Z. T. and Bernede, M. J. (1979) Suggested methods for determining the uniaxial compressive strength and deformability of rock materials, for ISRM Commission on Standardization of Laboratory and Field Tests, *Int. J. Rock Mech. Min. Sci.* **16** (2).

Bieniawski, Z. T. and Hawkes, I. (1978) Suggested methods for determining tensile strength of rock materials, for ISRM Commission on Standardization of Lab and Field Tests, *Int. J. Rock Mech. Min. Sci.* **15:** 99–104.

Bieniawski, Z. T. and Van Heerden, W. L. (1975) The significance of in-situ tests on large rock specimens, *Int. J. Rock Mech. Min. Sci.* **12:** 101–113.

Broch, E. (1974) The influence of water on some rock properties, *Proc. 3rd Cong. ISRM* (Denver), Vol. II A, pp. 33–38.

Brown, E. T., Richards, L. W., and Barr, M. V. (1977) Shear strength characteristics of Delabole slates, *Proceedings, Conference on Rock Engineering* (British Geotechnical Society, Vol. 1, pp. 33–51.

Cook, N. G. W. and Hodgson, K. (1965) Some detailed stress-strain curves for Rock, *J. Geophys. Res.* **70:** 2883–2888.